



1,3-Dipolar cycloaddition to the Fe–S=C fragment 20. Preparation and properties of carbonyliron complexes of di-thiooxamide. Reactivity of the mononuclear (di-thiooxamide)Fe(CO)₃ towards dimethyl acetylenedicarboxylate

Ron Siebenlist^a, Hans-Werner Frühauf^{a,*}, Huub Kooijman^b, Nora Veldman^b, Anthony L. Spek^b, Kees Goubitz^a, Jan Fraanje^a

^a *Universiteit van Amsterdam, Institute of Molecular Chemistry, Anorganisch Chemisch Laboratorium, Nieuwe Achtergracht 166, 1018 WV Amsterdam, The Netherlands*

^b *Bijvoet Center for Biomolecular Research, Crystal and Structural Chemistry, Utrecht University, Padualaan 8, 3584 CH Utrecht, The Netherlands*

Received 17 April 2001; accepted 29 August 2001

Dedicated to Professor Kees Vrieze

Abstract

Reaction of Fe₂(CO)₉ at room temperature in THF with the di-thiooxamides (L), S=C{N(R,R')}–C{(R,R')N}–S [R = Me, R'–R' = (CH₂)₂ (**a**); R = H, R' = ⁱPr (**b**); R = H, R' = ⁱiPr (**c**), R = H, R' = benzyl (**d**); R = H, R' = H (**e**)], results for ligands **a–d** initially in the formation of the mononuclear σ-S, σ-S' chelate complexes Fe(CO)₃(L) (**7a–d**), which could be isolated in case of **7a** and **7d**. Under the reaction conditions, complexes **7a–d** react further with [Fe(CO)₄] fragments to give three types of Fe₂(CO)₆(L) complexes (**8a–d**) in high yields, depending on the di-thiooxamide ligand used together with traces of the known complex S₂Fe₃(CO)₉ (**14**). The molecular structures of these complexes have been established by the single crystal X-ray diffraction determinations of **8a**, **8b** and **8d**. In the reaction with ligand **e** the corresponding complex **7e** was not detected and the well-known complexes **14** and S₂Fe₃(CO)₉ (**15**) were isolated in low yield. In situ prepared **7a** reacts in a slow reaction with 1 equiv. of dimethyl acetylene dicarboxylate in a 1,3-dipolar cycloaddition reaction to give the stable initial ferra [2.2.1] bicyclic complex **10a** in 60% yield. In complex **10a** an additional Fe(CO)₄ fragment is coordinated to the sulfido sulfur atom of the cycloadded Fe–S=C fragment. When a toluene solution of **10a** is heated to 50 °C it loses two terminal CO ligands to give the binuclear Fe–Fe bonded complex **11a** in almost quantitative yield. The molecular structures of **10a** and **11a** have been confirmed by single crystal X-ray diffraction. Reaction of **7d** at room temperature with 2 equiv. of dimethyl acetylene dicarboxylate results in the mononuclear complex **12d** in 5% yield. The molecular structure of **12b** has been established by single crystal X-ray diffraction and comprises a tetra dentate ligand with two ferra-sulpha cyclobutene, and a ferra-disulpha cyclopentene moiety. When the reaction is performed at 60 °C a low yield of 2,3,4,5-thiophene tetramethyl tertracarboxylate is obtained besides complex **12d**. © 2002 Elsevier Science B.V. All rights reserved.

Keywords: Crystal structures; Cycloaddition; Iron complexes; Carbonyl complexes; Thiooxamide complexes

Abbreviations: R-DAB, 1,4-diaza-1,3-butadienes of formula R¹N=C(H)–C(H)=NR¹; DMAD, dimethyl acetylene dicarboxylate; MP, methyl propynoate; AIB(R¹,E,E'), the organic ligand resulting from C–C bond formation between an R-DAB ligand and an alkyne EC≡CE'. The backbone of the ligand is R¹N=C(H)C(H)(NR¹)C(E)=CE', which is 3-amino-4-imino-1-butene.

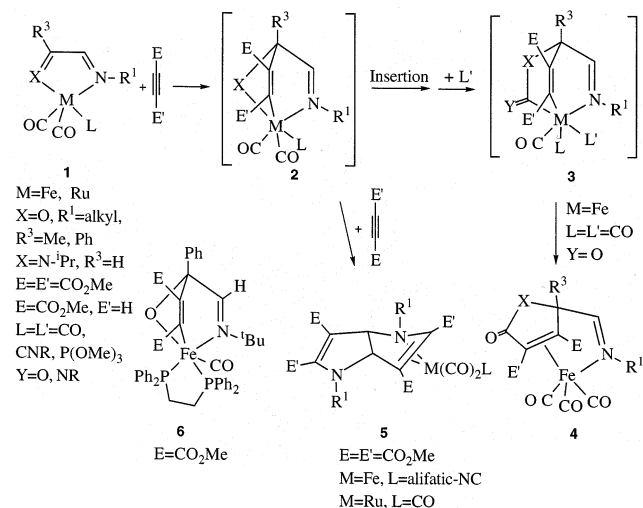
* Corresponding author. Tel.: +31-20-525 6458; fax: +31-20-525 6456.

E-mail address: hwf@science.uva.nl (H.-W. Frühauf).

1. Introduction

In the last decade, the reactions of the mononuclear $M(\text{CO})_n(\text{CNR})_{3-n}(\text{R-DAB})$ complexes ($M = \text{Fe}, \text{Ru}$; $n = 0, 1, 3$) [1–8] with the alkynes DMAD and MP have been studied extensively in our laboratory. These reactions have been shown to give some interesting highly functionalised coordinated heterocyclic ligands such as in complexes **4** and **5** (cf. Scheme 1). It has been demonstrated in the previous parts of this series that the initial step in these reactions consists of a 1,3-dipolar cycloaddition reaction of the activated alkyne (dipolarophile) across the $M\text{--}N\text{=C}$ fragment (1,3-dipole), resulting in the formation of the bicyclo [2.2.1] intermediate **2**. In order to extend the synthetic potential of this reaction we studied the reaction of the isostructural mononuclear $\text{Fe}(\text{CO})_3(\text{N}\alpha\text{O})$ ($\text{N}\alpha\text{O} = \alpha\text{-iminoketone}$ and $\alpha\text{-iminoester}$) complexes and found that they react via a similar reaction sequence [9,10]. This was proven by the solid state structure of the initial bicyclo[2.2.1] $\text{Fe}(\text{Ph}_2\text{PCH}_2\text{CH}_2\text{PPh}_2)(\text{CO})$ adduct **6** [11] and the isolation of the stable adducts **2** (cf. Scheme 1; $X = \text{O}, \text{L} = \text{PR}_3$).

To further exploit this reaction we recently directed our interest to the N,N' di- and tetra-substituted di-thiooxamides (abbreviated as $\text{R}_2\text{-DTO}$ and $\text{R}_4\text{-DTO}$, respectively). The objective was to synthesise mononuclear chelate $\sigma\text{-S}, \sigma\text{-S}'$ $\text{Fe}(\text{CO})_3(\text{DTO})$ complexes and to probe their reactivity towards DMAD. The X-ray structures of several $\text{R}_2\text{-DTO}$ ligands ($\text{R} = \text{Et}, \text{}^i\text{Pr}, \text{H}$) [12,13] showed that they consist of two C–C coupled



Scheme 1. Reactions of $\text{Fe}(\text{CO})_2\text{L}(\text{R}^1\text{-DAB})$ and $\text{Fe}(\text{CO})_3(\alpha\text{-iminoketone})$ with electron-deficient alkynes.

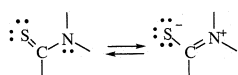


Fig. 1. Resonance structure of thioamide fragment.

almost perfectly planar and rigid thioamide functions in a planar $E\text{-}s\text{-}trans\text{-}E$ geometry (cf. Fig. 2; **b,c,e**). In case of $\text{Et}_4\text{-DTO}$ [14], the two thioamide groups are almost orthogonal (dihedral angle around $\text{SC}\text{--}\text{CS} = 89.8^\circ$) in the solid state due to steric hindrance of the ethyl groups. The quite perfect sp^2 geometry of nitrogen evidences the strong electron delocalisation within the $\text{N}\text{--}\text{C}\text{--}\text{S}$ moiety (cf. Fig. 1), which is characterised by longer C–S and shorter C–N bond lengths with respect to the usual value for the corresponding un-conjugated bonds. The long central C–C bond reveals that there is no net delocalisation of the π -electrons over both thioamide groups.

A large number of papers have been published concerning transition metal complexes with di-thiooxamide ligands [14–21]. However, in only a few of them the di-thiooxamide is coordinated as a neutral bidentate $\sigma\text{-S}, \sigma\text{-S}'$ ligand in a $s\text{-}cis$ conformation and without hydrogen bonds to other, e.g. halide, ligands. Furthermore, the crystal structures of $\text{Zn}(\text{Me}_2\text{-DTO})\text{Cl}_2$ [16], $\text{Cu}(\text{Bzl}_2\text{-DTO})_2[\text{ClO}_4]_2$ [16], and particularly $\text{Re}(\text{CO})_3\text{Br}(\text{Et}_4\text{-DTO})$ [21] show that these ligands do not possess a planar geometry when they are S, S' -coordinated to a metal centre in a $s\text{-}cis$ conformation. A planar co-ordination is precluded by the steric interactions between, respectively, the amide protons or the ethyl groups on the rigid sp^2 nitrogen, which results in dihedral angles around the central C–C bond of approximately 36 and 77° , respectively.

In the earlier parts of this series we have reported on the 1,3-dipolar cycloadditions of $M(\text{CO})_n(\text{CNR})_{3-n}(\text{R-DAB})$ ($M = \text{Fe}, \text{Ru}$; $n = 0, 1, 3$) and $\text{Fe}(\text{CO})_n(\text{PR}_3)_{3-n}(\text{N}\alpha\text{O})$ ($\text{N}\alpha\text{O} = \alpha\text{-iminoketone}$ and $\alpha\text{-iminoesters}$; $n = 0, 1, 2$) complexes. From these investigations two important conditions with respect to the 1,3-dipolar reactivity emerged; (i) since the $\text{Fe}\text{--}\text{X}\text{=C}$ ($X = \text{NR}, \text{O}$) fragment can be classified as nucleophilic type I 1,3-dipole [22–27], a relatively high electron density is required [1,6,8,10,28–30], and (ii) because the cycloaddition proceeds over the $\text{Fe}\text{--}\text{X}\text{=C}$ ($X = \text{NR}, \text{O}$) fragment, the metal atom must be able to increase its co-ordination number and oxidation state.

As has been shown, the 1,3-dipolar cycloadditions proceed readily with 1,4-dihetero-1,3-diene ligands (D-DAB , $\alpha\text{-imino-ketone}$ and esters) which possess a low lying π^* -orbital in combination with the electron rich metals $\text{Fe}(0)$ and $\text{Ru}(0)$. Apparently, strong π -back donation of the metal into the $\pi^*\text{-LUMO}$ of these ligands activates the $\text{Fe}\text{--}\text{X}\text{=C}$ ($X = \text{O}, \text{NR}$) fragment for cycloaddition reactions. Consequently, our aim was to synthesise five-co-ordinate d^8 -metal complexes with a $\sigma\text{-S}, \sigma\text{-S}'$ chelate DTO ligand in which a synergism of π -back donation and flattening of the $\text{S}\text{--}\text{C}\text{--}\text{S}$ backbone would lower the LUMO energy and populate the π^* -level sufficiently for 1,3-dipolar cycloaddition across the $\text{Fe}\text{--}\text{S}\text{=C}$ fragment.

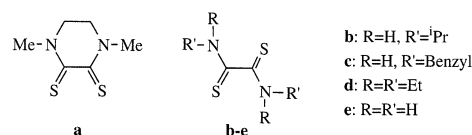


Fig. 2. Structures and geometry of DTO ligands.

The co-ordination behaviour of several R_2 - and R_4 -DTO ligands to $Mo(CO)_{4-n}(PR_3)_n$ has been studied by tom Dieck et al. [18,19]. For $n=0, 1$, they found that the DTO ligand acts as a relatively strong donor and for $n=2$, the R_2 - and R_4 -DTO ligand acts as good π -acceptor ligand. Obviously, the electron density on the Mo centre is sufficiently increased by the two phosphorus ligands to cause extensive π -back donation into the π^* -LUMO, which results in a planar S–C–C–S skeleton. Servaas et al. [21] have shown and supported by MO-calculations that the decrease in the dihedral angle of the cyclic DTO ligand *N,N'*-dimethylpiperazine-2,3-dithione (*cyclo*-DTO; Fig. 2(a)) from 35.4° (free ligand) to 18° in (*cyclo*-DTO) $Re(CO)_3Br$ is the result of π -back donation from the metal in to the π^* -LUMO of the *cyclo*-DTO ligand. The central C–C bond is accordingly shortened because the π^* -orbital is bonding between these two carbons. This shortening of the central C–C bond is also found in the solid state structures of $Fe(CO)_3(R-DAB)$ [31,32] complexes and $Fe(CO)_3(MeN=C(Ph)-C(Ph)=O)$ [33].

The five DTO ligands used in this investigation are shown in Fig. 2. The cyclic DTO ligand **a** is used because it already has a *cis* arrangement, and no steric hindrance between the thioamide functions is expected. As representatives for the R_2 -DTO and R_4 -DTO ligands, we have used iPr_2 -DTO (**b**), benzyl $_2$ -DTO (**c**) and Et_4 -DTO (**d**), respectively. Finally, di-thiooxamide (**e**) is also used.

The reactions of ligands **a–e** with $Fe_2(CO)_9$ are investigated. In the case of ligands **a–d**, initially, the deep green or blue $Fe(CO)_3(DTO)$ complexes (**7**) are observed before they react further with $[FeCO]_4$ to three different types of $Fe_2(CO)_6(DTO)$ complexes **8**. The reactions of **7a** and **7d** with DMAD have been studied.

2. Experimental

2.1. General information

1H and ^{13}C NMR spectra were recorded on a Bruker AMX-300 spectrometer. The IR spectra were recorded on a Biorad FTIR-7 spectrophotometer. Elemental analyses were carried out by Dornis and Kolbe, Microanalytisches Laboratorium, Mülheim a. d. Ruhr, Germany and by the University of Amsterdam. The solvents were carefully dried and distilled under nitrogen prior to use. All preparations were carried out

under an atmosphere of dry nitrogen by conventional Schlenk techniques. Silicagel for column chromatography (Kieselgel 60, 70-230 mesh, E. Merck, Darmstadt, Germany) was dried and activated prior to use by heating to $160^\circ C$ under vacuum for 16 h. $Fe(CO)_5$ (Strem Chemicals), DMAD (Janssen) and di-thiooxamide (Janssen) were used as commercially obtained. $Fe_2(CO)_9$ [34]¹ has been prepared according to the published procedure. The ligands *cyclo*-DTO [35] (**a**), R_2 -DTO (**b, c**) [36] and Et_4 -DTO (**d**) [36] were prepared according to published procedures.

2.2. Synthesis of $Fe(CO)_3(cyclo-DTO)$ (**7a**)

To a stirred suspension of 1.092 g (3.00 mmol) $Fe_2(CO)_9$ in 40 ml of THF an amount of 486 mg (3.00 mmol) of *cyclo*-DTO (**a**) was added, whereupon the solution immediately turned deep blue (**7a**). After all the $Fe_2(CO)_9$ had been consumed (± 45 min), the deep blue coloured solution was evaporated to dryness and the residue was redissolved in 60 ml of pentane/ Et_2O (1:1) (**7a**) and filtered. Cooling the pentane/ Et_2O solution of **7a** to $-30^\circ C$ resulted in dark blue–purple lustrous micro crystalline material of $Fe(CO)_3(cyclo-DTO)$ (**7a**) in about 40% yield together with small amounts ($< 5\%$) of the dimeric $Fe_2(CO)_6(cyclo-DTO)$ (**8a**). Unfortunately, these crystals were not suitable for X-ray diffraction. Subsequent crystallisation from the concentrated mother liquor at $-30^\circ C$ led to a second batch of crystalline material of **7a** (20%), giving a total yield of about 60% (based on the amount of *cyclo*-DTO used).

2.3. Synthesis of $Fe(CO)_3(Et_4-DTO)$ (**7d**)

To a stirred suspension of 1.092 g (2.00 mmol) $Fe_2(CO)_9$ in 40 ml of THF an amount of 696 mg (3.00 mmol) of Et_4 -DTO (**d**) was added, whereupon the solution turned deep green–blue (**7d**) within 3 min. After all the $Fe_2(CO)_9$ had been consumed (± 30 min), the deep green coloured solution was evaporated to dryness and the residue was redissolved in 60 ml of pentane and filtered. Cooling the pentane solution to $-30^\circ C$ resulted in a voluminous precipitate of the excess free Et_4 -DTO ligand. Filtration gave a deep green–blue solution containing a mixture of the mononuclear complex $Fe(CO)_3(Et_4-DTO)$ (**7d**) and the

¹ $Fe_2(CO)_9$ was prepared by a slightly modified literature procedure using a quartz Schlenk tube and starting with 25 ml $Fe(CO)_5$, 150 ml glacial acetic acid and 10 ml acetic anhydride (the latter was added to prevent the mixture containing too much water). A rayonet RS photochemical reactor ($\lambda_{max} = 2500 \text{ \AA}$) was used for irradiation and a continuous stream of air was used to cool the reaction mixture. Filtration, washing with water, ethanol, ether, and subsequently drying in vacuo gave $Fe_2(CO)_9$ in usually more than 90% yield.

dimeric complex $\text{Fe}_2(\text{CO})_6(\text{Et}_4\text{-DTO})$ (**8d**) in a ratio of approximately 2:1, in a total yield of about 50% (based on the amount of $\text{Et}_4\text{-DTO}$ used).

2.4. Synthesis of $\text{Fe}_2(\text{CO})_6(\text{DTO})$ (**8a–d**)

2.4.1. Reaction in THF

To a stirred suspension of 1.820 g (5 mmol) $\text{Fe}_2(\text{CO})_9$ in 40 ml of THF an amount of 2.00 mmol of the respective DTO ligand was added [324 mg (**a**); 408 mg (**b**); 600 mg (**c**) and 464 mg (**d**)], whereupon the solution turned deep blue (**a**), or deep green–blue (**b–d**). The reaction mixture was stirred for 3 h during which time the colour of the reaction mixture changed from dark blue–green to dark brown. After evaporation of the solvent the residue was redissolved in a minimum of CH_2Cl_2 and the products were separated by column chromatography on silicagel (column 1×15 cm).

In all cases, elution with pentane/ Et_2O (19:1) afforded a reddish-brown fraction from which after evaporation of the solvent the known complex $\text{Fe}_3(\text{CO})_9\text{S}_2$ (**14**) [37] could be obtained as a dark brown powder in approximately 2% yield. Reaction with ligand **a**: further elution with $\text{Et}_2\text{O}/\text{CH}_2\text{Cl}_2$ (9:1) afforded a dark brown fraction which after evaporation of the solvent gave $\text{Fe}_2(\text{CO})_6(\text{cyclo-DTO})$ (**8a**) as a brown powder in 70% yield. Crystals of **8a** suitable for X-ray diffraction were obtained by slow addition of CH_2Cl_2 to a suspension of **8a** in Et_2O until the product was completely dissolved, followed by cooling to -60°C for 2 days. Reaction with ligands **b,c**: further elution with pentane/ Et_2O (1:1) afforded an orange–brown fraction which after evaporation of the solvent gave $\text{Fe}_2(\text{CO})_6(\text{R}_2\text{-DTO})$ (**8b,c**) as dark orange–brown oils in about 80% yield. Complexes **8b, c** dissolve very well in pentane and could not be crystallised from this solvent. Crystals of **8b** suitable for X-ray diffraction were obtained by cooling a concentrated EtOH solution (500 mg in 2 ml) of **8b** to -60°C for several weeks. Reaction with ligand **d**: further elution with pentane/ Et_2O (3:1) afforded a dark reddish-black fraction which after evaporation of the solvent gave $\text{Fe}_2(\text{CO})_6(\text{Et}_4\text{-DTO})$ (**8d**) as a dark black powder in about 90% yield. Black crystals of **8d** suitable for X-ray diffraction were obtained from a saturated EtOH solution made at room temperature and then cooled to $+4^\circ\text{C}$.

2.4.2. Reaction in toluene

The reactions in toluene were performed as in THF only taking 16 instead of 3 h. The yields were lower; 35% (**8a**) and 70% (**7a–d**). In the case of the reaction of *cyclo*-DTO (**a**), a new product was formed. Elution with Et_2O afforded an orange fraction, which after evaporation of the solvent yielded the dimeric complex **9** as an orange oil in about 2% yield. Crystals of **9** suitable for X-ray diffraction were obtained by cooling a pentane solution to -60°C for several weeks.

2.5. Reaction of $\text{Fe}_2(\text{CO})_9$ with di-thiooxamide (**e**)

To a stirred suspension of 1.820 g (5 mmol) $\text{Fe}_2(\text{CO})_9$ in 40 ml of THF an amount of 240 mg (2.00 mmol) di-thiooxamide (**e**) was added. The reaction mixture was stirred until all $\text{Fe}_2(\text{CO})_9$ had reacted (± 3 h), during which time the colour of the reaction mixture had changed to dark brown. The reaction mixture was evaporated to dryness and the products were separated by column chromatography on silicagel (column 1×15 cm). Elution with pentane/ Et_2O (19:1) afforded a reddish-brown fraction which, after evaporation of the solvent, gave a mixture of the known complexes $\text{Fe}_3(\text{CO})_9\text{S}_2$ (**14**) and $\text{Fe}_2(\text{CO})_6\text{S}_2$ (**15**) (3:1) as a dark brown powder in approximately 4% yield.

2.6. Synthesis of complexes **10a** and **11a** by in situ reaction of **7a** with DMAD

To a stirred suspension of 2.548 g (7.00 mmol) $\text{Fe}_2(\text{CO})_9$ in 40 ml of THF an amount of 486 mg (3.00 mmol) *cyclo*-DTO was added, whereupon the solution immediately turned deep blue indicating the formation of $\text{Fe}(\text{CO})_3(\text{cyclo-DTO})$ (**7a**). Immediately a solution of 381 μl (3.1 mmol) DMAD in 20 ml of THF was added dropwise at such a rate (ca. 1 drop/3 s) that the solution stayed light green. During the reaction the solution became dark brown and when all the $\text{Fe}_2(\text{CO})_9$ had reacted, the reaction mixture was stirred for another 30 min. The IR spectrum of the reaction mixture showed only the CO stretching bands of complex **10a**. After evaporation of the solvent, the remaining dark brown oily residue was redissolved in 5 ml of CH_2Cl_2 and the product was purified by column chromatography on silicagel (column 1×15 cm). Elution with Et_2O gave a yellow fraction containing impurities. Subsequent elution with $\text{Et}_2\text{O}/\text{CH}_2\text{Cl}_2$ (2:1) afforded a reddish brown to brown fraction, which after evaporation of the solvent gave a mixture of **10a** and **11a** (6:1) as a red–brown powder in a total yield of about 60%. Since **10a** and **11a** could not be separated by column chromatography on silicagel they were separated by crystallisation. Deep red–brown crystals of **10a** suitable for X-ray diffraction were obtained by slow addition of CH_2Cl_2 to a suspension of the mixture of products in Et_2O , followed by cooling to -60°C for 2 days in about 80% yield (based on the weight of the column fraction).

Because it was not possible to separate the two products remaining in the red brown mother liquor, it was stirred in toluene at 50°C to convert **10a** in **11a**. The reaction was monitored by IR spectroscopy and was stopped when the CO stretching bands of **10a** had been completely converted into those of **11a**, during which time the colour of the solution changed from red brown to brown. Complex **11a** can also be obtained

from pure **10a** by stirring it at 50 °C in toluene. Crystals of **11a** suitable for X-ray diffraction were obtained by slowly adding CH₂Cl₂ to a suspension of Et₂O until a clear solution was obtained, followed by cooling to –60 °C for 1 week.

2.7. Reaction of Fe(CO)₃(cyclo-DTO) (**7a**) with DMAD

To a dark blue solution of 628 mg (2.00 mmol) Fe(CO)₃(cyclo-DTO) (**7a**) in 40 ml of THF a solution of 246 μl (2.00 mmol) DMAD in 15 ml of THF was added in one lot. The reaction was followed by IR spectroscopy. The IR-bands of the starting complex **7a** disappeared during approximately 1 h, however, only a minute amount of a defined product (<5% of **10a**) could be isolated by column chromatography.

2.8. Reaction of **10a** with CO

(a) A stirred toluene or THF solution of **10a** was placed under an atmosphere of CO at room temperature. The reaction was followed by IR spectroscopy and no change could be detected after several days. Heating the solution to 50 °C resulted in the formation of **11a**.

(b) A toluene solution of **10a** was placed in an autoclave under 20 bars of CO. The reaction was followed by IR spectroscopy and revealed that **10a** slowly decomposes and no other complexes were detected.

2.9. Reaction of **10a** with MeI

A weighted amount of **10a** was dissolved in toluene or THF and an excess of MeI is added. The reaction was followed by IR spectroscopy and no change could be detected after several days.

2.10. Synthesis of **12d** and **13**

(a) To a solution containing approximately 1.00 mmol of Fe(CO)₃(Et₄-DTO) (**7d**) (see above) in 30 ml of hexane was added 492 μl (4 mmol) DMAD at room temperature. The reaction was followed by IR spectroscopy. Complete conversion of Fe(CO)₃(Et₄-DTO) (**7d**) took approximately 2 weeks during which time the colour of the reaction mixture changed from deep green–blue to dark brown–black. After evaporation of the solvent, the remaining red–brown oily residue was redissolved in 3 ml of CH₂Cl₂ and the product was purified by column chromatography on silicagel. Elution with pentane/Et₂O (1:1) afforded a dark brown–black fraction which after evaporation of the solvent gave Fe₂(CO)₆(Et₄-DTO) (**8d**) and free DMAD as a dark brown–black oil. Subsequent elution with Et₂O/CH₂Cl₂ (9:1) afforded an orange–red fraction which

after evaporation of the solvent gave **12d** as a red oil in about 5% yield. Red–orange crystals of **12d** suitable for X-ray diffraction were obtained by slow addition of CH₂Cl₂ to a suspension of **12d** in pentane, followed by cooling to –60 °C for 2 days.

(b) The reaction was performed analogous to **a**, only at 60 °C. On column chromatography, elution with Et₂O afforded an orange–red fraction which after evaporation of the solvent gave a mixture of **12d** and **13** as a mixture of red and white powders in a total yield of 7%, in a ratio of approximately 1:1. When the obtained mixture of **12d** and **13** was stirred at 60 °C with DMAD the ratio did not change.

(c) The reaction was performed in THF as described above. However, no detectable amounts of either **12d** or **13** were formed.

2.11. Reaction of Fe₂(CO)₆(Et₄-DTO) (**8d**) with DMAD

To an amount of 512 mg (1.00 mmol) **8d** in 20 ml of hexane or THF was added 492 μl (4 mmol) DMAD at room temperature or 60 °C. The reaction was followed by IR spectroscopy and no change could be detected after several days.

2.12. Crystal structure determinations of **8a**, **8d**, **10a**, **11a** and **12d**

Crystals suitable for X-ray diffraction were glued to the tip of a glass fibre and transferred into the cold nitrogen stream on an Enraf–Nonius CAD4-T diffractometer on rotating anode. Accurate unit-cell parameters and an orientation matrix were determined by least-squares fitting of the setting angles of a set of well-centred reflections (SET4) [38]. Reduced-cell calculations did not indicate higher lattice symmetry [39]. Crystal data and details on data collection and refinement are collected in Table 1. All data were collected in ω–2θ scan mode.

Data were corrected for *Lp* effects and for the observed linear decay of the reference reflections. An empirical absorption correction was applied for all compounds except for **12d** (DIFABS) [40].

The structures of all compounds were solved by automated Patterson methods and subsequent difference Fourier techniques (SHELXS86 [41] for **8a** and DIRDIF-92 [42] for the other complexes). All structures were refined on *F*² using full-matrix least-squares techniques (SHELXL-93) [43]; no observance criterion was applied during refinement on *F*². Hydrogen atoms were included in the refinement on calculated positions, riding on their carrier atoms. All methyl hydrogen atoms were refined in a rigid group, allowing for rotation around the C–C, N–C or C–O bonds. The non-hydrogen atoms of all structures were refined with an-

Table 1
Crystal data and details of the structure determination of **8a**, **8b**, **8d**, **10a**, **11a** and **12d**

Compound	8a	8b	8d
<i>Crystal data</i>			
Empirical formula	C ₁₂ H ₁₀ Fe ₂ N ₂ O ₆ S ₂	C ₁₄ H ₁₆ Fe ₂ N ₂ O ₆ S ₂	C ₁₆ H ₂₀ Fe ₂ N ₂ O ₆ S ₂
Formula weight	454.05	430.0	512.17
Crystal system	monoclinic	triclinic	triclinic
Space group	<i>P</i> 2 ₁ / <i>c</i> (No. 14)	<i>P</i> $\bar{1}$ (No. 2)	<i>P</i> $\bar{1}$ (No. 2)
<i>a</i> (Å)	9.9573(6)	8.938(1)	8.460(3)
<i>b</i> (Å)	10.7268(6)	9.603(2)	11.377(3)
<i>c</i> (Å)	15.2144(9)	12.359(3)	11.814(5)
α (°)	90	88.15(2)	71.97(3)
β (°)	95.902(5)	74.18(2)	81.32(3)
γ (°)	90	88.92(2)	86.26(3)
<i>V</i> (Å ³)	1616.44(16)	1020.0(5)	1068.7(7)
<i>Z</i>	4	4	2
<i>D</i> _{calc} (g cm ⁻³)	1.866	1.50	1.592
<i>F</i> (000) (electrons)	912	492	524
μ (cm ⁻¹)	20.7 [Mo K α]	136.5 [Cu K α]	15.9 [Mo K α]
Crystal size (mm)	0.05 × 0.25 × 0.30	0.30 × 0.40 × 0.60	0.15 × 0.25 × 0.35
<i>Data collection</i>			
Temperature (K)	150	228	150
θ_{\min} , θ_{\max} (°)	2.1, 27.5	3.7, –75.1	1.8, 27.5
SET4 θ_{\min} , θ_{\max} (°)	10.19, 13.95 [25 refl]	40, 43 [23 refl]	9.82, 15.03 [25 refl]
Wavelength (Å)	0.71073 [Mo K α]	1.54184 [Cu K α]	0.71073 [Mo K α]
Filter/monochromator	graphite mon.	graphite mon.	graphite mon.
$\Delta\omega$ (°)	0.63 + 0.35 tan θ	1.2 + 0.15 tan θ	1.65 + 0.35 tan θ
Horizontal and vertical aperture (mm)	2.17, 4.00	3.00, 1.00	4.15, 4.00
X-ray exposure time (h)	15	48	20
Linear instability (%)	2	5	3
Reference reflections	2 2 4, –4 2 1, –1 5 1	0 0 3, 0 2 0	–2 1 –4, –2 2 –4, 0 –2 2
Dataset	–12:12, 0:13, –17:19	–11:0, –12:12, –15:14	–10:0, –14:14, –15:14
Total data	6643	4202	4737
Total unique data	3684	4202	4415
<i>R</i> _{int}	0.023		0.093
Observed data	[no crit applied]	2771 [<i>I</i> > 2.5 σ (<i>I</i>)]	[no crit applied]
Absorption correction range (DIFABS)	0.90, 1.09	0.15, 2.24	0.65, 1.61
<i>Refinement</i>			
Number of refined parameters	219		257
Final <i>R</i> ₁ ^a	0.0335 [3005 <i>I</i> > 2 σ (<i>I</i>)]	0.107 [<i>I</i> > 2.5 σ (<i>I</i>)]	0.0569 [2803 <i>I</i> > 2 σ (<i>I</i>)]
Final <i>wR</i> ₂ ^b	0.0819		0.1363
Final <i>Rw</i>		0.147	
Goodness-of-fit	1.029		0.966
<i>w</i> ⁻¹ ^c	$\sigma^2(F^2) + (0.0398P)^2 + 1.32P$	$3.0 + F + 0.013F^2$	$\sigma^2(F^2) + (0.0692P)^2$
(Δ/σ) _{av} , (Δ/σ) _{max}	0.000, 0.014	0.000, 0.97	0.000, 0.001
Minimum and maximum resd. dens. (e Å ⁻³)	–0.58, 0.78	–2.9, 2.3	–0.58, 0.78
	10a	11a	12d
<i>Crystal data</i>			
Empirical formula	C ₁₉ H ₁₆ Fe ₂ N ₂ O ₁₁ S ₂	C ₁₇ H ₁₆ Fe ₂ N ₂ O ₉ S ₂ ·CH ₂ Cl ₂	C ₂₄ H ₃₂ FeN ₂ O ₁₀ S ₂
Formula weight	624.17	653.08	628.50
Crystal system	triclinic	monoclinic	monoclinic
Space group	<i>P</i> 1 (No.2)	<i>P</i> 2 ₁ / <i>c</i> (No. 14)	<i>Cc</i> (No. 9)
<i>a</i> (Å)	11.450(2)	14.9993(9)	13.3849(11)
<i>b</i> (Å)	14.4347(13)	10.2231(7)	19.267(2)
<i>c</i> (Å)	15.490(2)	18.9091(13)	11.5416(9)
α (°)	93.109(10)	90	90
β (°)	103.116(12)	120.417(5)	107.515(6)
γ (°)	93.771(10)	90	90
<i>V</i> (Å ³)	2481.7(6)	2500.4(3)	2838.4(4)
<i>Z</i>	4	4	4
<i>D</i> _{calc} (g cm ⁻³)	1.671	1.735	1.471
<i>F</i> (000) (electrons)	1264	1320	1312

Table 1 (Continued)

Compound	8a	8b	8d
μ (cm ⁻¹)	13.9 [Mo K α]	15.9 [Mo K α]	7.3 [Mo K α]
Crystal size (mm)	0.15 \times 0.15 \times 0.45	0.05 \times 0.15 \times 0.35	0.15 \times 0.20 \times 0.80
<i>Data collection</i>			
Temperature (K)	150	150	150
θ_{\min} , θ_{\max} (°)	1.4, 27.5	1.6, 27.5	1.9, 27.5
SET4 θ_{\min} , θ_{\max} (°)	11.58, 13.88 [25 refl]	9.93, 13.87 [25 refl]	9.86, 14.04 [25 refl]
Wavelength (Å)	0.71073 [Mo K α]	0.71073 [Mo K α]	0.71073 [Mo K α]
Filter/monochromator	graphite mon.	graphite mon.	graphite mon.
$\Delta\omega$ (°)	0.73 + 0.35 tan θ	0.55 + 0.35 tan θ	0.72 + 0.35 tan θ
Horizontal and vertical aperture (mm)	2.62, 4.00	3.00, 4.00	3.04, 4.00
X-ray exposure time	24	20	17
Linear instability (%)	2	3	1
Reference reflections	-2 1 5, 3 2 2, -2 4 2	-2 3 1, 0 2 5, 5 1 2	2 -2 -3, 4 -2 -6, -5 -5 2
Dataset	-14:13, -18:18, 0:19	-19:17, -13:0, -21:24	-17:17, -24:0, -14:14
Total data	10 845	10 023	6946
Total unique data	10 454	5726	6462
R_{int}	0.061	0.045	0.019
Observed data	[no crit applied]	[no crit applied]	[no crit applied]
Absorption correction range	0.86, 1.20	0.92, 1.07	
<i>Refinement</i>			
Number of refined parameters	657	320	361
Final R_1 ^a	0.0577 [6559I > 2 σ (I)]	0.0488 [3710I > 2 σ (I)]	0.0407 [5178I > 2 σ (I)]
Final wR_2 ^b	0.1252	0.0964	0.0907
Final R_w			
Goodness-of-fit	0.992	0.964	1.030
w^{-1} ^c	$\sigma^2(F^2) + (0.0510P)^2$	$\sigma^2(F^2) + (0.0327P)^2$	$\sigma^2(F^2) + (0.0432P)^2 + 1.05P$
$(\Delta/\sigma)_{\text{av}}$, $(\Delta/\sigma)_{\text{max}}$	0.000, 0.005	0.000, 0.001	0.000, 0.001
Minimum and maximum res. dens. (e Å ⁻³)	-0.55, 0.56	-0.53, 0.77	-0.30, 0.33

$$^a R_1 = \frac{\sum |F_o| - |F_c|}{\sum |F_o|}$$

$$^b wR_2 = \frac{[\sum (w(F_o^2 - F_c^2)^2)] / \sum (w(F_o^2)^2)]^{1/2}}$$

$$^c P = (\max(F_o^2, 0) + 2F_c^2) / 3$$

isotropic parameters. The hydrogen atoms were refined with a fixed isotropic parameter related to the value of the equivalent isotropic displacement parameter of their carrier atoms by a factor of 1.5 for the methyl hydrogen atoms and 1.2 for the other hydrogen atoms.

Compound **12d** contains a pseudo inversion centre at [0.486, 0.000, 0.227]. Refinement in the centric space group $C2/c$ (No. 15) leads to considerably higher R -values ($wR_2 = 0.19$, $R_1 = 0.07$) and introduces conformational disorder in the ester groups containing C(2) and C(21) and, to a lesser degree, also in the N -ethyl groups. Refinement in spacegroup Cc gives a complete ordered model with no residual density above 0.2 Å⁻³ near the ester groups. The Flack x parameter [44], derived during the structure factor calculation, amounted to a value of 0.72(2), indicating a possible racemic twin. Refinement of a racemic twin model resulted in better wR_2 -values and a component ratio of 0.28(2):0.72.

Neutral atom scattering factors and anomalous dispersion corrections were taken from the International Tables for Crystallography [45]. Geometrical calculations and illustrations were performed with PLATON

[46], all calculations were performed on a DEC station 5000 cluster.

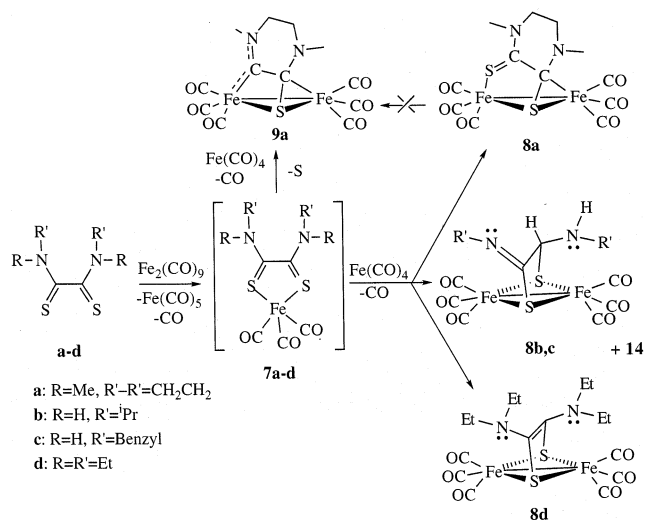
2.13. X-ray structure determination of **8b**

A crystal with dimensions 0.30 \times 0.40 \times 0.60 mm was used for data collection on an Enraf–Nonius CAD-4 diffractometer with graphite-monochromated Cu K α radiation and ω - 2θ scan. A total of 4202 unique reflections was measured, of which 2771 were above the significance level of 2.5 σ (I). The maximum value of $(\sin\theta)/\lambda$ was 0.63 Å⁻¹. Two reference reflections were measured hourly and showed a decrease of 5% during the 48 h collecting time, which was corrected for. Unit-cell parameters were refined by a least-square fitting procedure using 23 reflections with $80 < 2\theta < 86^\circ$. Corrections for Lorentz and polarisation effects were applied. The structure was solved by the PATTY/ORIENT/PHASEX option of the DIRDIF91 [47] programme system. The hydrogen atoms were calculated. Full-matrix least-squares refinement on F , anisotropic for the non-hydrogen atoms and isotropic for the hydrogen atoms, restraining the latter in such a way that

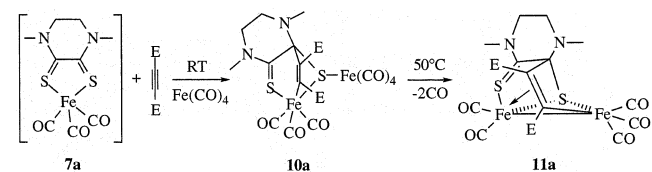
the distance to their carrier remained constant at approximately 1.09 Å, converged $R = 0.107$, $R_w = 0.147$, $(\Delta/\sigma)_{\max} = 0.97$. An empirical absorption correction was applied (DIFABS) [40]. A final Fourier map revealed a residual electron density in the vicinity of the heavy atoms. Scattering factors were taken from Cromer and Mann [48]; International Tables for X-ray Crystallography [49]. The anomalous scattering of Fe and S was taken into account. All calculations were performed with XTAL [50], unless stated otherwise.

3. Results and discussion

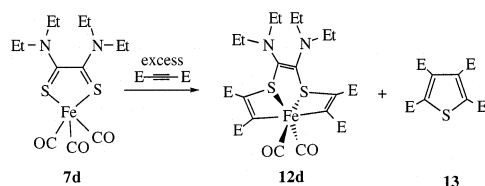
The complexes discussed in this investigation are schematically presented in Schemes 2–4, and the ligands are shown in Fig. 2. The types of complexes are identified by Arabic numbers.



Scheme 2. Reactions of the di-thioamide ligands **a–d** with $\text{Fe}_2(\text{CO})_9$.



Scheme 3. Reaction of $\text{Fe}(\text{CO})_3(\text{cyclo-DTO})$ (**7a**) with DMAD.



Scheme 4. Reaction of $\text{Fe}(\text{CO})_3(\text{Et}_4\text{-DTO})$ with DMAD.

3.1. Synthesis of mononuclear $\sigma\text{-S}$, $\sigma\text{-S}'$ chelate complexes $\text{Fe}(\text{CO})_3(\text{DTO})$ (**7**) and the dimeric complexes $\text{Fe}_2(\text{CO})_6(\text{DTO})$ (**8a–d**)

Reaction of $\text{Fe}_2(\text{CO})_9$ with the DTO ligands **a–d** in THF at room temperature results in all cases initially in the formation of the deep blue–green coloured mononuclear chelate $\text{Fe}(\text{CO})_3(\alpha\text{-iminoketone})$ complexes (**7a–d**). However, only with the ligands **a** and **d** complexes **7** are reasonably stable under the reaction conditions and can be isolated in moderate (**7a**; 60%) and low (**7d**; 38%) yield. Complex **7d** is isolated as a mixture together with the dimeric complex **8d** (see Section 2). Complexes **7a,d** have been characterised spectroscopically (IR, UV–Vis, ¹H NMR, ¹³C NMR, FD-mass) and by elemental analysis of **7a**.

In the case of the reaction with ligands **b** and **c**, the initial deep green–blue $\text{Fe}(\text{CO})_3(\text{DTO})$ complexes **7b,c** are formed in low stationary concentrations because they directly react further with $[\text{Fe}(\text{CO})_4]$ to form the dimeric $\text{Fe}_2(\text{CO})_6[\text{R}'\text{N}=\text{C}(\text{S})-(\text{S})\text{C}(\text{H})\text{N}(\text{H})\text{R}']$ complexes **8b,c** in high yield. The two sulfur atoms of the modified DTO ligand in complexes **8b,c** are reduced to sulfido groups which are bridging between the two $\text{Fe}(\text{CO})_3$ fragments ($\mu_2\text{-S}$ co-ordination), thus acting as a six-electron donor. In complexes **8b,c**, one of the amide protons has undergone a 1,3-H shift to the carbon atom of the other thioamide moiety with formation of a new imine function. The proposed structure was confirmed by a single crystal X-ray diffraction analysis of complex **8b**. Also the mononuclear complexes **7a,d** react with $[\text{Fe}(\text{CO})_4]$ to form the dimeric complexes **8a,d**, however, they both differ structurally from **7b,c**. Reaction of **7a** with $[\text{Fe}(\text{CO})_4]$ results in the formation of $\text{Fe}_2(\text{CO})_6(\text{cyclo-DTO})$ (**8a**) in good yield. The *cyclo-DTO* ligand in **8a** is $\sigma\text{-S}$, $\mu_2\text{-S}'$, $\eta^2\text{-C}=\text{S}'$ coordinated, donating six electrons to the metal centres, which is confirmed by a single crystal X-ray structure determination of **8a**. This type of co-ordination is well known and observed in many other $\text{M}_2(\text{CO})_6(\text{L})$ complexes ($\text{M} = \text{Fe}, \text{Ru}, \text{FeRu}$; $\text{L} = \text{R-DAB}$ [51–54], $\alpha\text{-iminoketone}$ [33] and $\alpha\text{-iminoester}$ [55]). When the reaction of **a** with $\text{Fe}_2(\text{CO})_9$ is performed in toluene instead of THF, a new dimeric complex (**9a**) is formed in very low yield besides **8a**. The molecular structure of **9a** is established by single crystal X-ray structure determination. Reaction of **8a** in toluene at room temperature or 70 °C does not result in a detectable amount of **9a**, indicating that **9a** is not formed from **8a**. However, since the structure of complex **9a** is beyond the scope of this thesis, the characterisation and the X-ray crystal structure determination will be reported elsewhere.

Reaction of **7d** with $[\text{Fe}(\text{CO})_4]$ results in the formation of $\text{Fe}_2(\text{CO})_6(\text{Et}_4\text{-DTO})$ (**8d**). In complex **8d** both the reduced sulfido atoms of the DTO ligand are $\mu_2\text{-S}$ coordinated between two $\text{Fe}(\text{CO})_3$ fragments donating six electrons to the metal centres, analogous to **8b,c**.

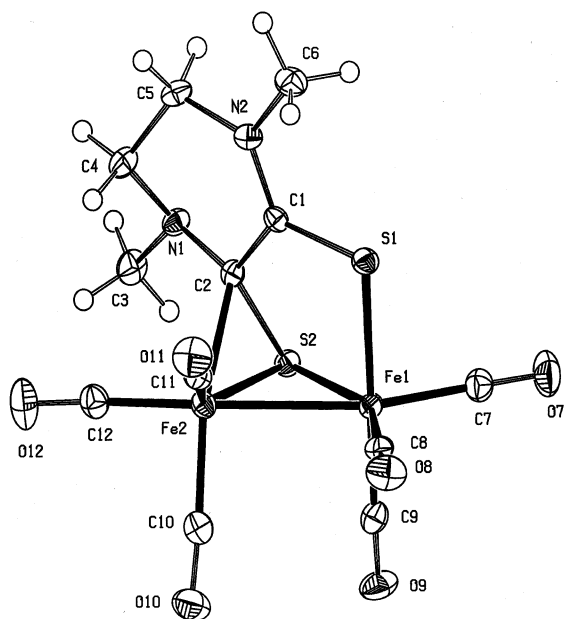


Fig. 3. ORTEP drawing (50% probability level) of the molecular structure of **8a**.

The molecular structure of **8d** is confirmed by single crystal X-ray determination. Complexes **8** are further characterised spectroscopically and by elemental analyses. Reaction of $\text{Fe}_2(\text{CO})_9$ with di-thiooxamide (**e**) does not result in a detectable concentration of $\text{Fe}(\text{CO})_3$ -(DTO) (**7e**); instead, the known complexes $\text{Fe}_3(\text{CO})_9\text{S}_2$ (**14**) [37] and $\text{Fe}_2(\text{CO})_6\text{S}_2$ (**15**) [56] are formed in low yield.

3.2. Reactions of **7a** with DMAD

In situ prepared mononuclear $\text{Fe}(\text{CO})_3(\text{cyclo-DTO})$ (**7a**) reacts in a slow reaction at room temperature with 1 equiv. of DMAD to give the initial bicyclo[2.2.1] cycloadduct **10a** as a result of a 1,3-dipolar cycloaddition reaction across the Fe-S=C fragment (cf. Scheme 3). From the IR data it is evident that **10a** contains two carbonyl iron moieties in different oxidation states since the six observed CO stretching bands cover a range from 2095 to 1928 cm^{-1} . The structure is confirmed by a single crystal X-ray structure determination, which showed that an additional $\text{Fe}(\text{CO})_4$ unit is coordinated to the sulfido sulfur atom. Reaction of isolated **7a** with 1 equiv. of DMAD also gives **10a**, however, in very low yield. The additional $\text{Fe}(\text{CO})_4$ unit is supplied by partial decomposition. The co-ordination of $\text{Fe}(\text{CO})_4$ is obviously essential to stabilise the bicyclo[2.2.1] structure which otherwise decomposes. Attempts to displace the σ -S coordinated $\text{Fe}(\text{CO})_4$ unit from **10a** with either CO (1 bar) or by oxidative addition of MeI, to study the further reaction, failed because no reaction was detected. Reaction under higher pressures of CO (20 bar) leads to decomposition.

When a solution of **10a** is heated in toluene to 50 °C it reacts further to the dinuclear Fe–Fe bonded complex **11a**. Complex **11a** is also formed to a small extent upon purification of **10a** on silicagel (see Section 2). The molecular structure of **11a** is confirmed by a single crystal X-ray structure determination. Closely related complexes have been observed in the in situ 1,3-dipolar cycloaddition reactions of $\text{Fe}(\text{CO})_3(\text{L})$ ($\text{L} = \alpha$ -iminoketone [57], α -iminoester [58]) with DMAD (cf. Fig. 8) and in the reactions of $\text{M}_2(\text{CO})_6(\text{R-DAB})$ ($\text{M} = \text{FeRu}$, Ru_2) with DMAD and other alkynes [59–61].

3.3. Reactions of **7d** with DMAD

When a mixture of the mononuclear $\text{Fe}(\text{CO})_3(\text{Et}_4\text{-DTO})$ (**7d**) and the dimer $\text{Fe}_2(\text{CO})_6(\text{Et}_4\text{-DTO})$ (**8d**) is reacted at room temperature with 4 equiv. of DMAD, the mononuclear complex **12d** is obtained in a very slow reaction in only 5% yield (cf. Scheme 4).

Because pure **8d** does not react with DMAD at room temperature in hexane, **12d** must originate from the reaction of **7d** and DMAD. From the IR, FD-mass and ^1H NMR spectra it is clear that complex **12d** is mononuclear and contains 2 equiv. of DMAD. The molecular structure has been determined by single crystal X-ray structure analysis. Reaction at 60 °C in hexane gives, as well as **12d**, the thiophene derivative **13** in low yield ($\pm 3\%$). When complex **12d** is reacted with DMAD at 60 °C, no observable reaction is detected, indicating that **13** is not formed from **12d**. Furthermore, **13** is not formed by the reaction of DMAD with either **8d** or free ligand (**d**). Apparently, in the reaction of **7d** with DMAD the reaction co-ordinate branches at some stage, producing either **12d** or **13**, or a totally different reaction path is followed.

3.4. Molecular structure of $\text{Fe}_2(\text{CO})_6(\text{cyclo-DTO})$ (**8a**)

An ORTEP drawing of the molecular structure of **8a** together with the atomic numbering scheme is shown in Fig. 3. Selected bond lengths and angles are given in Table 2.

The structure consists of two inequivalent $\text{Fe}(\text{CO})_3$ units which are linked by an Fe–Fe metal bond and bridged by a σ -S, μ_2 -S', η^2 -C=S' coordinated *cyclo*-DTO ligand, which donates six electrons to the metal centres. All CO ligands are terminally bonded with normal bond distances and angles. The Fe–Fe bond distance ($\text{Fe}(1)\text{--Fe}(2) = 2.6714(6)$ Å) compares well with the values of 2.671(1) and 2.705(1) Å reported for $\text{Fe}_2(\text{CO})_6[\text{SCS}(\text{CH}_2)_2\text{S}]$ [62] and $\text{Fe}_2(\text{CO})_6[\text{SC}(\text{Ph})\text{C}(\text{O})\text{SMe}]$ [62], which both contain a similar mono μ_2 -S bridge, and falls within the range of 2.50–2.70 Å [63] for a normal Fe–Fe single bond. Compared to the Fe–Fe bond distances of the isostructural complexes $\text{Fe}_2(\text{CO})_6(\text{L})$ ($\text{L} = \text{PhCH}(\text{Me})\text{N}=\text{C}(\text{H})\text{C}(\text{OEt})=\text{O}$ [64],

Table 2
Selected bond distances (Å) and angles (°) for **8a** (e.s.d.s in parentheses)

Bond distances					
Fe(1)–Fe(2)	2.6714(6)	Fe(2)–S(2)	2.1850(8)	S(2)–C(2)	1.757(3)
Fe(1)–S(1)	2.2864(8)	Fe(2)–C(2)	2.149(3)	N(1)–C(2)	1.418(4)
Fe(1)–S(2)	2.2242(8)	Fe(2)–C(10)	1.795(3)	N(1)–C(3)	1.454(4)
Fe(1)–C(7)	1.810(3)	Fe(2)–C(11)	1.791(3)	N(2)–C(1)	1.325(4)
Fe(1)–C(8)	1.813(3)	Fe(2)–C(12)	1.783(3)	N(2)–C(6)	1.457(4)
Fe(1)–C(9)	1.792(3)	S(1)–C(1)	1.713(2)	C(1)–C(2)	1.462(4)
Bond angles					
Fe(1)–S(1)–C(1)	101.48(11)	C(5)–N(2)–C(6)	115.8(2)	N(1)–C(2)–C(1)	114.1(2)
Fe(1)–S(2)–Fe(2)	74.58(3)	S(1)–C(1)–N(2)	119.1(2)	N(1)–C(4)–C(5)	109.3(2)
Fe(1)–S(2)–C(2)	100.03(11)	S(1)–C(1)–C(2)	120.1(2)	N(2)–C(5)–C(4)	111.1(2)
Fe(2)–S(2)–C(2)	65.02(10)	N(2)–C(1)–C(2)	120.8(2)	Fe(1)–C(7)–O(7)	179.0(3)
C(2)–N(1)–C(3)	119.5(2)	Fe(2)–C(2)–S(2)	67.16(11)	Fe(1)–C(8)–O(8)	177.8(3)
C(2)–N(1)–C(4)	111.8(2)	Fe(2)–C(2)–N(1)	123.4(2)	Fe(1)–C(9)–O(9)	176.6(3)
C(3)–N(1)–C(4)	113.6(2)	Fe(2)–C(2)–C(1)	108.5(2)	Fe(2)–C(10)–O(10)	176.5(3)
C(1)–N(2)–C(5)	122.5(2)	S(2)–C(2)–N(1)	117.5(2)	Fe(2)–C(11)–O(11)	178.9(3)
C(1)–N(2)–C(6)	121.5(2)	S(2)–C(2)–C(1)	118.3(2)	Fe(2)–C(12)–O(12)	174.9(3)

hex-DAB [51]) the Fe–Fe bond in **8a** is somewhat elongated, which is probably due to the bigger radius of sulfur compared to that of nitrogen. The Fe(1)–S(2) and Fe(2)–S(2) bond distances of 2.2242(8) and 2.1850(8) Å, respectively, and the Fe(1)–S(2)–Fe(2) angle of 74.58(3)°, compare well with those reported for Fe₂(CO)₆(SC(Ph)C(O)SMe), which contains a ligand with a similar σ-S, μ₂-S', η²-C=S' co-ordination. The Fe(2)–C(2) σ-bond (2.149(3) Å) in **8a** is somewhat longer than the corresponding bond of 2.110(4) Å in the latter complex. The Fe(1)–S(1) σ-bond of 2.2864(8) Å is somewhat shorter than those in **10a** (2.3170(14) Å), **11a** (2.3087(11) Å), and other σ-S Fe(CO)₃ [65] complexes, which may be due to the rigidity of the cyclo-DTO ligand. Due to its π-co-ordination, the C(2)=S(2) bond (1.757(3) Å) is significantly elongated compared to the mean C=S bond distance of 1.664(4) Å found in the free ligand [21]. The N(1)–C(2) bond (1.418(4) Å) is also significantly elongated compared to the mean value of 1.326(4) Å reported for the free ligand, because the conjugation within the N(1)–C(2)–S(1) moiety is lost (cf. Fig. 1). The S(1)=C(1) double bond (1.713(2) Å) is only slightly elongated due to co-ordination to iron, and the C(1)–N(2) bond length (1.325(4) Å) is almost equal to that in the free ligand, indicating that the N(2)–C(1)–S(1) thioamide fragment is still fully conjugated. This is reflected in the sp² hybridisation of N(2). The sum of the angles around N(2) is 359.8(3)° and the atoms N(2), C(1), S(1) and C(2) are almost coplanar (largest deviation: C(2) = 0.004(3) Å). The sum of the angles around N(1) amounts to 344.9(3) Å.

3.5. Molecular structure of

Fe₂(CO)₆[ⁱPrN=C(S)–(S)C(H)N(H)ⁱPr] (**8b**)

An ORTEP drawing of the molecular structure of **8b** together with the atomic numbering scheme is shown in

Fig. 4. Selected bond lengths and angles are given in Table 3.

Although the high *R*-value (0.107) of structure **8b** does not warrant a detailed discussion, the structure is clear. Complex **8b** consists of two inequivalent Fe(CO)₃ fragments held together by two *S*-sulfido bridges (μ₂-coordinated) of the modified ⁱPr₂-DTO ligand, which donate six electrons to the metal centres and a normal Fe–Fe single bond of 2.504(3) Å. The Fe(1)–Fe(2) bond length compares very well with the values found for many other complexes containing a similar Fe₂(CO)₆–(μ₂-S)₂ moiety, e.g. 2.502(1) Å in [Fe(CO)₃(SCH₂)₂]₂ [66], 2.507(5) Å in [Fe(CO)₃SC(C₆H₅)₂]₂ [67], and 2.495(3) Å in [Fe(CO)₃(μ₂-SPh)]₂ [68]. Also the mean Fe–S bond distances (2.254(4) Å) and the mean Fe–S–Fe bond angles (67.5(1)°) of the Fe₂(CO)₆(μ₂-S)₂ moiety in **8b** are almost equal to corresponding bond lengths and angles reported for [Fe(CO)₃(SCH₂)₂]₂, [Fe(CO)₃SC(C₆H₅)₂]₂ and [Fe(CO)₃(μ₂-SPh)]₂. As a result of the 1,3-H shift of the amide proton from N(1) to C(2), the N(1)–C(1) bond is oxidised to an imine double bond which is

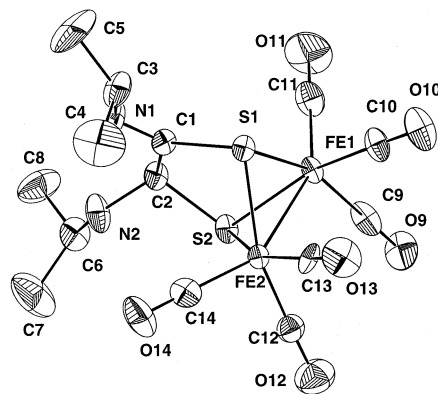


Fig. 4. ORTEP drawing (30% probability level) of the molecular structure of **8b**.

Table 3
Selected bond distances (Å) and angles (°) for **8b** (e.s.d.s in parentheses)

Bond distances					
Fe(1)–Fe(2)	2.504(3)	Fe(2)–S(1)	2.268(3)	S(1)–C(1)	1.80(1)
Fe(1)–S(1)	2.251(3)	Fe(2)–S(2)	2.253(3)	S(2)–C(2)	1.85(1)
Fe(1)–S(2)	2.243(3)	Fe(2)–C(12)	1.73(1)	N(1)–C(1)	1.25(2)
Fe(1)–C(9)	1.79(1)	Fe(2)–C(13)	1.81(1)	N(2)–C(2)	1.42(2)
Fe(1)–C(10)	1.78(1)	Fe(2)–C(14)	1.79(1)	C(1)–C(2)	1.51(2)
Fe(1)–C(11)	1.79(1)				
Bond angles					
Fe(1)–S(1)–Fe(2)	67.3(1)	Fe(2)–S(2)–C(2)	102.7(4)	N(1)–C(1)–C(2)	120(1)
Fe(1)–S(1)–C(1)	106.2(4)	C(1)–N(1)–C(3)	123(1)	S(2)–C(2)–N(2)	110(1)
Fe(2)–S(1)–C(1)	98.0(4)	C(2)–N(2)–C(6)	116(1)	S(2)–C(2)–C(1)	109.9(8)
Fe(1)–S(2)–Fe(2)	67.7(1)	S(1)–C(1)–N(1)	125(1)	N(2)–C(2)–C(1)	110(1)
Fe(1)–S(2)–C(2)	104.2(4)	S(1)–C(1)–C(2)	115.0(9)		

reflected in the N(1)=C(1) bond distance of 1.25(1) Å. This is confirmed by the sum of the angles around C(1) which amounts to 360(1)°, indicating sp² hybridisation. The different hybridisations (sp² and sp³) of carbons C(1) and C(2) probably account for the difference in bonding distances to the respective sulfur atoms, 1.80(1) and 1.85(1) Å, respectively.

3.6. Molecular structure of

$\text{Fe}_2(\text{CO})_6[(\text{Et})_2\text{N}-\text{C}(\text{S})=\text{S})\text{C}-\text{N}(\text{Et})_2]$ (**8d**)

An ORTEP drawing of the molecular structure of **8d** together with the atomic numbering scheme is shown in Fig. 5. Selected bond lengths and angles are given in Table 4.

The molecule of **8d** consists of two identical $\text{Fe}(\text{CO})_3$ units held together by two μ_2 -bridging sulfido groups of the reduced Et₄-DTO ligand which donate six electrons to the metal centres, and an Fe–Fe bond. The molecule exhibits non-crystallographic twofold rotation symmetry with the rotation axis running through the centres of the C(1)=C(2) and the Fe(1)–Fe(2) bonds. All the CO ligands are terminally bonded with normal bond distances and angles. The Fe(1)–Fe(2) bond distance of 2.4805(15) Å compares very well with that in **8b**, and those of the other complexes discussed earlier containing a similar $\text{Fe}_2(\text{CO})_6(\mu_2\text{-S})_2$ skeleton. The four Fe–S bond distances vary from 2.2439(1) to 2.265(2) Å, and the two Fe–S–Fe bond angles are 66.67(6) and 66.81(6)° for S(1) and S(2), respectively. These bond distances and angles are, as expected, again almost equal to those in $[\text{Fe}(\text{CO})_3\text{SC}(\text{C}_6\text{H}_5)]_2$ [67], $[\text{Fe}(\text{CO})_3(\text{SCH}_2)]_2$ [66], $[\text{Fe}(\text{CO})_3(\mu_2\text{-SPh})]_2$ [68], and **8b**. As a result of the reduction of both the sulfur atoms, the central C(1)–C(2) bond is oxidised to a double bond (1.341(8) Å). This bond length is comparable with the corresponding C=C bond length of 1.350 Å in $[\text{Fe}(\text{CO})_3\text{SC}(\text{C}_6\text{H}_5)]_2$ [67]. The two C(1)–S(1) and C(2)–S(2) bond distances (1.817(6) Å and 1.800(5) Å, respectively) are slightly different and compare well

with those in $[\text{Fe}(\text{CO})_3(\text{SCH}_2)]_2$ and $[\text{Fe}(\text{CO})_3\text{-SC}(\text{C}_6\text{H}_5)]_2$. Though in solution all corresponding nuclei in the two molecular halves are equivalent in ¹H and ¹³C NMR down to 163 K, in the crystal structure, the C(1)–N(1) (1.366(8) Å) and C(2)–N(2) (1.415(7) Å) bond distances differ significantly, indicating partial double bond character for the C(1)–N(1) bond. This is corroborated by the sum of the angles around N(1) of 359.9(8)° which indicates sp² hybridisation while the sum of the angles around N(2) is 339.7(8)°, indicative of a hybridisation in between sp² and sp³. Furthermore, the sp² character of N(1) is supported by the coplanarity of S(1), S(2), C(1), C(2) and N(1) [largest deviation; C(2) = 0.053(5) Å] with N(2) 0.267(4) Å from this plane. The difference in geometry of N(1) and N(2) is probably due to packing effects in the crystal lattice.

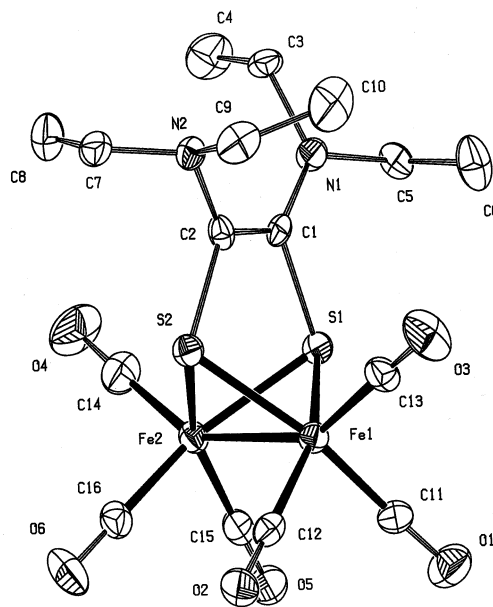


Fig. 5. ORTEP drawing (50% probability level) of the molecular structure of **8d**. Hydrogen atoms are omitted for clarity.

Table 4
Selected bond distances (Å) and angles (°) for **8d** (e.s.d.s in parentheses)

Bond distances					
Fe(1)–Fe(2)	2.4805(15)	Fe(2)–S(1)	2.265(2)	S(1)–C(1)	1.817(6)
Fe(1)–S(1)	2.2483(18)	Fe(2)–S(2)	2.2439(18)	S(2)–C(2)	1.800(5)
Fe(1)–S(2)	2.262(2)	Fe(2)–C(14)	1.796(6)	N(1)–C(1)	1.366(8)
Fe(1)–C(11)	1.779(6)	Fe(2)–C(15)	1.784(6)	N(2)–C(2)	1.415(7)
Fe(1)–C(12)	1.795(6)	Fe(2)–C(16)	1.786(6)	C(1)–C(2)	1.341(8)
Fe(1)–C(13)	1.789(6)				
Bond angles					
Fe(1)–S(1)–Fe(2)	66.67(6)	C(2)–N(2)–C(9)	112.6(4)	N(1)–C(5)–C(6)	112.4(5)
Fe(1)–S(1)–C(1)	104.0(2)	C(7)–N(2)–C(9)	111.9(5)	N(2)–C(7)–C(8)	111.9(5)
Fe(2)–S(1)–C(1)	102.02(19)	S(1)–C(1)–N(1)	115.0(4)	N(2)–C(9)–C(10)	111.1(5)
Fe(1)–S(2)–Fe(2)	66.81(6)	S(1)–C(1)–C(2)	114.3(4)	Fe(1)–C(11)–O(1)	178.2(5)
Fe(1)–S(2)–C(2)	102.73(19)	N(1)–C(1)–C(2)	130.7(5)	Fe(1)–C(12)–O(2)	179.1(5)
Fe(2)–S(2)–C(2)	103.70(19)	S(2)–C(2)–N(2)	117.1(4)	Fe(1)–C(13)–O(3)	178.7(5)
C(1)–N(1)–C(3)	121.3(4)	S(2)–C(2)–C(1)	115.3(4)	Fe(2)–C(14)–O(4)	178.2(6)
C(1)–N(1)–C(5)	121.6(5)	N(2)–C(2)–C(1)	127.4(5)	Fe(2)–C(15)–O(5)	178.7(5)
C(3)–N(1)–C(5)	117.0(5)	N(1)–C(3)–C(4)	111.3(5)	Fe(2)–C(16)–O(6)	177.7(5)
C(2)–N(2)–C(7)	115.2(4)				

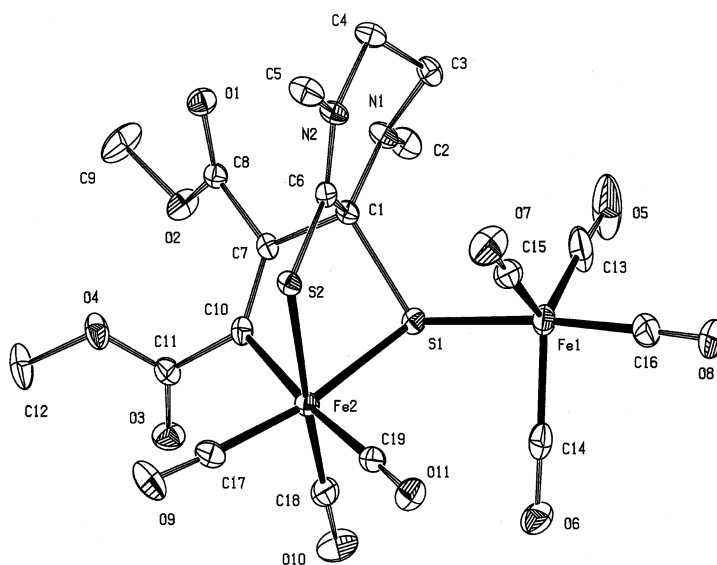


Fig. 6. ORTEP drawing (30% probability level) of the molecular structure of **10a**. Hydrogen atoms are omitted for clarity and only one of the two crystallographically independent molecules is shown.

3.7. Molecular structure of [2.2.1] bicyclic complex **10a**

An ORTEP drawing of the molecular structure of **10a** together with the atomic numbering scheme is shown in Fig. 6. Selected bond lengths and angles are given in Table 5. The asymmetric unit of the unit cell contains two crystallographically independent molecules. Numbers in brackets refer to the corresponding geometrical parameters in the second molecule.

The molecular structure of **10d** consists of an Fe(2) centre coordinated by a newly formed [2.2.1] bicyclic structure, in which the Fe(2) and the former thiocarbonyl carbon C(1) occupy the bridgehead positions, and three terminal CO ligands. Furthermore, an Fe(1)(CO)₄ fragment is coordinated to the sulfido atom

S(1). The co-ordination geometry around the central Fe(2) atom is distorted octahedral as a consequence of its [2.2.1] bicyclic structure. The [2.2.1] bicyclic terdentate ligand is not able to span three regular octahedral co-ordination sites (S(2)–Fe(2)–C(10) = 87.68(13)° [87.18(13)°], S(2)–Fe(2)–S(1) = 87.14(5)° [87.42(5)°] and S(1)–Fe(2)–C(10) = 80.32(14)° [81.29(14)°]). These angles are less distorted from an ideal octahedral geometry than those of the isostructural [2.2.1] iron [11,69] (e.g. **6** in Scheme 1) and ruthenium [7] complexes.

As a result of the 1,3-dipolar cycloaddition reaction over the Fe–S=C fragment, the S(1)–C(1) bond is reduced to a single bond of 1.905(5) Å [1.881(5) Å], which compares well with the value of 1.910(5) Å for the corresponding S–C(sp³) bond in **11a**. The C(1)–N(1)

bond is also elongated to 1.412(6) Å [1.417(7) Å] compared with the C–N distance in free DTO which clearly shows that the N(1)–C(1)–S(1) moiety is not conjugated anymore. The S(2)–C(6) and C(6)–N(2) bond distances of 1.694(5) Å [1.691(5) Å] and 1.292(6) Å [1.303(6) Å], respectively, are comparable with the corresponding bond distances reported for several free DTO ligands [12,13,21], indicating that this thioamide moiety is still fully delocalised. The C(7)–C(10) bond of the former alkyne has been reduced to a double bond of 1.329(6) Å [1.324(6) Å], and C(10) is σ -bonded to iron by a bond of 1.997(5) Å [1.998(5) Å]. Both these bond distances are similar to those found in two isostructural iron [2.2.1] bicyclic structures [11,69]. The Fe(2)–S(2) σ -donative bond distance of 2.3170(14) Å [2.3116(15) Å] is comparable with that in **11a** and several other σ -donative S–Fe(CO)₃ bond distances reported in the literature [65]. The sulfido sulfur atom S(1) is σ -bonded to Fe(2) by a bond of 2.2851(14) Å [2.2880(15) Å] and bonded to Fe(1) by a σ -donative bond of 2.2950(14) Å [2.3117(14) Å], i.e. μ_2 -coordinated between Fe(1) and Fe(2). These bond distances are somewhat longer than those found in **8b,d**, because the two iron centres in **10a** are only bridged by one sulfido group. The co-ordination geometry of Fe(1) is trigonal bipyramidal (deviation; 4.6% [10.4%]) along the Berry pseudo rotation

co-ordinate) [70], with the sulfur donor S(1) in an apical position [71].

The most important result in the context of this paper, however, is the observation of the [2.2.1] bicyclic structure, which proves that the Fe–S=C fragment reacts with DMAD in a 1,3-dipolar cycloaddition.

3.8. Molecular structure of **11a**

An ORTEP drawing of the molecular structure of **11a** together with the atomic numbering scheme is shown in Fig. 8. Selected bond distances and angles are given in Table 6.

The molecular structure of **11a** consists of an Fe(CO)₃ and an Fe(CO)₂ fragment held together by a metal–metal bond and a newly formed bridging eight electron donating ligand. All CO ligands are terminally bonded with normal bond lengths and angles. The new ligand results from C–C bond formation between one of the alkyne DMAD carbons (C(9)) and the former thiocarbonyl carbon atom C(1) of the *cyclo*-DTO ligand. Similar C–C connecting reactions have been observed in the in situ cycloaddition reactions of Fe(CO)₃(α -iminoketone) and Fe(CO)₃(α -iminoester) with DMAD (cf. Fig. 7) resulting in Fe₂(CO)₅(OIB) [58] (A) and Fe₂(CO)₅(OPP) [57] (B) complexes. Reaction of

Table 5
Selected bond distances (Å) and angles (°) for **10a** (e.s.d.s in parentheses)

Bond distances					
Fe(1)–S(1)	2.2950(14)	Fe(2)–C(18)	1.811(6)	N(2)–C(5)	1.475(6)
Fe(1)–C(13)	1.794(6)	Fe(2)–C(19)	1.829(5)	N(2)–C(6)	1.292(6)
Fe(1)–C(14)	1.786(6)	S(1)–C(1)	1.905(5)	C(1)–C(6)	1.531(6)
Fe(1)–C(15)	1.784(6)	S(2)–C(6)	1.694(5)	C(1)–C(7)	1.532(7)
Fe(1)–C(16)	1.772(6)	N(1)–C(1)	1.412(6)	C(3)–C(4)	1.508(7)
Fe(2)–S(1)	2.2851(14)	N(1)–C(2)	1.458(6)	C(7)–C(8)	1.476(6)
Fe(2)–S(2)	2.3170(14)	N(1)–C(3)	1.432(6)	C(7)–C(10)	1.329(6)
Fe(2)–C(10)	1.997(5)	N(2)–C(4)	1.478(6)	C(10)–C(11)	1.480(7)
Fe(2)–C(17)	1.818(6)				
Bond angles					
S(1)–Fe(1)–C(13)	89.1(2)	S(2)–Fe(2)–C(19)	87.63(14)	S(1)–C(1)–C(6)	106.6(3)
S(1)–Fe(1)–C(14)	83.69(17)	C(10)–Fe(2)–C(17)	90.1(2)	S(1)–C(1)–C(7)	100.4(3)
S(1)–Fe(1)–C(15)	94.9(2)	C(10)–Fe(2)–C(18)	89.8(2)	N(1)–C(1)–C(6)	112.6(4)
S(1)–Fe(1)–C(16)	174.0(2)	C(10)–Fe(2)–C(19)	173.7(2)	N(1)–C(1)–C(7)	113.2(4)
C(13)–Fe(1)–C(14)	116.7(3)	C(17)–Fe(2)–C(18)	95.2(3)	C(6)–C(1)–C(7)	107.4(4)
C(13)–Fe(1)–C(15)	122.1(3)	C(17)–Fe(2)–C(19)	94.1(2)	N(1)–C(3)–C(4)	107.5(4)
C(13)–Fe(1)–C(16)	91.7(3)	C(18)–Fe(2)–C(19)	94.6(2)	N(2)–C(4)–C(3)	109.1(4)
C(14)–Fe(1)–C(15)	121.2(3)	Fe(1)–S(1)–Fe(2)	120.11(5)	S(2)–C(6)–N(2)	122.1(4)
C(14)–Fe(1)–C(16)	90.7(3)	Fe(1)–S(1)–C(1)	118.93(15)	S(2)–C(6)–C(1)	117.4(3)
C(15)–Fe(1)–C(16)	89.6(3)	Fe(2)–S(1)–C(1)	91.35(15)	N(2)–C(6)–C(1)	120.5(4)
S(1)–Fe(2)–S(2)	87.14(5)	Fe(2)–S(2)–C(6)	101.43(16)	C(1)–C(7)–C(8)	116.3(4)
S(1)–Fe(2)–C(10)	80.32(14)	C(1)–N(1)–C(2)	118.0(4)	C(1)–C(7)–C(10)	118.4(4)
S(1)–Fe(2)–C(17)	169.73(18)	C(1)–N(1)–C(3)	118.1(3)	C(8)–C(7)–C(10)	123.9(4)
S(1)–Fe(2)–C(18)	88.39(19)	C(2)–N(1)–C(3)	118.2(4)	Fe(2)–C(10)–C(7)	117.4(3)
S(1)–Fe(2)–C(19)	95.17(15)	C(4)–N(2)–C(5)	115.2(4)	Fe(2)–C(10)–C(11)	119.8(3)
S(2)–Fe(2)–C(10)	87.68(13)	C(4)–N(2)–C(6)	123.2(4)	C(7)–C(10)–C(11)	122.7(4)
S(2)–Fe(2)–C(17)	88.90(18)	C(5)–N(2)–C(6)	121.6(4)	O(3)–C(11)–O(4)	123.2(4)
S(2)–Fe(2)–C(18)	175.18(18)	S(1)–C(1)–N(1)	115.6(3)	O(4)–C(11)–C(10)	112.0(4)

Table 6
Selected bond distances (Å) and angles (°) for **11a** (e.s.d.s in parentheses)

Bond distances					
Fe(1)–Fe(2)	2.5279(8)	Fe(2)–C(12)	1.943(5)	N(1)–C(4)	1.466(5)
Fe(1)–S(1)	2.2826(11)	Fe(2)–C(17)	1.809(5)	N(2)–C(1)	1.423(5)
Fe(1)–S(2)	2.3087(11)	Fe(2)–C(18)	1.798(4)	N(2)–C(5)	1.458(4)
Fe(1)–C(9)	2.104(4)	Fe(2)–C(19)	1.780(5)	N(2)–C(6)	1.455(5)
Fe(1)–C(12)	2.039(4)	S(1)–C(1)	1.910(5)	C(1)–C(2)	1.532(5)
Fe(1)–C(15)	1.795(5)	S(2)–C(2)	1.702(3)	C(1)–C(9)	1.513(5)
Fe(1)–C(16)	1.776(4)	N(1)–C(2)	1.304(4)	C(4)–C(5)	1.498(5)
Fe(2)–S(1)	2.2371(11)	N(1)–C(3)	1.466(5)	C(9)–C(10)	1.493(7)
Bond angles					
Fe(1)–C(9)–C(1)	92.9(3)	Fe(2)–S(1)–C(1)	104.71(11)	S(1)–C(1)–C(9)	99.1(3)
Fe(1)–C(9)–C(10)	118.8(2)	Fe(1)–S(2)–C(2)	93.20(12)	N(2)–C(1)–C(2)	113.1(3)
Fe(1)–C(9)–C(12)	67.7(2)	C(2)–N(1)–C(3)	121.3(3)	N(2)–C(1)–C(9)	115.5(3)
C(1)–C(9)–C(10)	118.0(3)	C(2)–N(1)–C(4)	121.8(3)	C(2)–C(1)–C(9)	107.9(3)
C(1)–C(9)–C(12)	121.6(4)	C(3)–N(1)–C(4)	116.7(3)	S(2)–C(2)–N(1)	123.5(3)
C(10)–C(9)–C(12)	119.6(3)	C(1)–N(2)–C(5)	112.5(3)	S(2)–C(2)–C(1)	115.1(2)
Fe(1)–C(12)–Fe(2)	78.77(17)	C(1)–N(2)–C(6)	114.9(3)	N(1)–C(2)–C(1)	121.4(3)
Fe(1)–C(12)–C(9)	72.7(2)	C(5)–N(2)–C(6)	112.7(3)	N(1)–C(4)–C(5)	111.6(3)
Fe(1)–C(12)–C(13)	130.8(2)	S(1)–C(1)–N(2)	119.1(3)	Fe(2)–C(12)–C(9)	122.7(3)
Fe(1)–S(1)–Fe(2)	68.01(3)	S(1)–C(1)–C(2)	100.2(3)	Fe(2)–C(12)–C(13)	117.1(3)
Fe(1)–S(1)–C(1)	77.97(11)	S(1)–C(1)–C(9)	99.1(3)	C(9)–C(12)–C(13)	119.3(4)

FeRu(CO)₆(R-DAB) with DMAD results in the formation of the analogous complex FeRu(CO)₆(AIB) [60]. The complexes A and B differ in their σ,π -co-ordination of the former alkyne DMAD. Complex **11a** is isostructural with complex B.

The Fe(1)–Fe(2) bond distance of 2.5279(8) Å is almost equal to the bond distance of 2.5257(10) Å found for complex B. In **11a** the sulfido atom S(1) is σ -bonded to Fe(1) (Fe(1)–S(1) = 2.2826(11) Å) and also bonded to Fe(2) via a σ -donative bond of 2.2371(11) Å, i.e. μ_2 -S bridging with an Fe(1)–S(1)–Fe(2) angle of 68.01(3)°. These Fe–S(1) bond distances are somewhat shorter (Fe(2)) and longer (Fe(1)) than the corresponding distances in **8b,d**, whereas the Fe(1)–S(1)–Fe(2) angle is almost equal to the Fe–S–Fe angles observed in **8b,d**. The ligand in **11a** is furthermore bonded to Fe(1) via S(2) and C(12). The Fe(1)–S(2) σ -donative bond distance of 2.3087(11) Å compares well with the one in **10a** of 2.3170(14) Å and other σ -donative (CO)₃Fe–S bond distances reported in the literature [65]. The Fe(1)–C(12) σ -bond of 1.943(5) Å is almost equal to the corresponding bond distances of 1.944(5), 1.950(11) and 1.955(5) Å in A, B and FeRu(CO)₆(AIB), respectively. The double bond C(9)–C(12) (1.405(5) Å) is elongated and rather asymmetrically coordinated to Fe(1) [Fe(1)–C(9) = 2.104(4) Å, Fe(1)–C(12) = 2.039(4) Å], a feature also observed in the co-ordination of the olefinic double bond in the related complexes A, B and FeRu(CO)₆(AIB). As a result of the C–C coupling on C(1), the C(1)–N(2) bond is elongated to 1.423(5) Å because it lost its conjugation with the C(1)–S(1) bond. The N(1)–C(2) and C(2)–S(2) bond distances of 1.304(4) and 1.702(3) Å indicate that this thioamide moiety is still delocalised.

3.9. Molecular structure of **12d**

An ORTEP drawing of the molecular structure of **12d** together with the atomic numbering scheme is shown in Fig. 9, and selected bond distances and angles are given in Table 7.

The molecular structure of **12d** consists of an Fe(II) centre coordinated by a newly formed dianionic ligand and two carbonyl ligands. The co-ordination around the central iron centre is distorted octahedral. This distortion is due to the formation of two four-membered rings, Fe(1)–C(1)–C(4)–S(1) and Fe(1)–C(20)–C(17)–S(2), which make an angle of 82.8(2)° with each other. The new ligand is coordinated to iron by two Fe(1)–S σ -donative bonds and two Fe(1)–C σ -bonds, and is probably formed by two successive insertions of the former DMAD triple bonds C(1)–C(4) and C(17)–C(20) in the Fe(1)–S(1) and Fe(1)–S(2) bonds, respectively. The Fe(1)–S(1) and Fe(1)–S(2) σ -donative bonds of 2.3356(14) and 2.3517(13) Å are slightly longer than those in **10a** and **11a**, which may be due to some strain in the four-membered rings. However, this is not reflected in the Fe(1)–C(1) and Fe(1)–C(20) bond distances (1.974(6) Å and 1.975(6) Å), which are

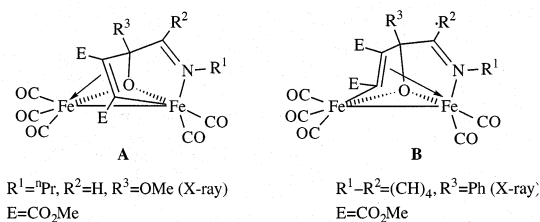


Fig. 7. Two complexes with a similar type of ligand as **11a**.

Table 7
Selected bond distances (Å) and angles (°) for **12d** (e.s.d.s in parentheses)

Bond distances					
Fe(1)–S(1)	2.3356(14)	S(1)–C(7)	1.786(6)	N(1)–C(7)	1.365(7)
Fe(1)–S(2)	2.3517(13)	S(2)–C(12)	1.784(5)	N(2)–C(12)	1.385(6)
Fe(1)–C(1)	1.974(6)	S(2)–C(17)	1.805(6)	C(1)–C(2)	1.468(7)
Fe(1)–C(20)	1.975(6)	O(9)–C(23)	1.157(7)	C(1)–C(4)	1.335(7)
Fe(1)–C(23)	1.766(6)	O(10)–C(24)	1.134(7)	C(4)–C(5)	1.494(7)
Fe(1)–C(24)	1.782(6)			C(7)–C(12)	1.383(8)
S(1)–C(4)	1.774(5)				
Bond angles					
S(1)–Fe(1)–S(2)	84.91(4)	C(20)–Fe(1)–C(24)	96.8(2)	C(13)–N(2)–C(15)	115.4(4)
S(1)–Fe(1)–C(1)	71.20(15)	C(23)–Fe(1)–C(24)	90.5(3)	Fe(1)–C(20)–C(17)	104.7(4)
S(1)–Fe(1)–C(20)	94.67(14)	Fe(1)–S(1)–C(4)	77.85(15)	Fe(1)–C(1)–C(4)	102.9(4)
S(1)–Fe(1)–C(23)	92.67(19)	Fe(1)–S(1)–C(7)	106.98(18)	C(2)–C(1)–C(4)	126.8(5)
S(1)–Fe(1)–C(24)	167.71(19)	C(4)–S(1)–C(7)	103.2(2)	S(1)–C(4)–C(1)	107.8(4)
S(2)–Fe(1)–C(1)	93.95(14)	Fe(1)–S(2)–C(12)	106.51(17)	S(1)–C(4)–C(5)	118.7(4)
S(2)–Fe(1)–C(20)	70.88(14)	Fe(1)–S(2)–C(17)	78.11(19)	C(1)–C(4)–C(5)	133.4(5)
S(2)–Fe(1)–C(23)	167.16(19)	C(12)–S(2)–C(17)	100.8(3)	S(1)–C(7)–N(1)	117.6(4)
S(2)–Fe(1)–C(24)	94.56(19)	C(7)–N(1)–C(8)	124.6(4)	S(1)–C(7)–C(12)	118.0(4)
C(1)–Fe(1)–C(20)	160.49(16)	C(7)–N(1)–C(10)	116.5(4)	S(2)–C(12)–N(2)	117.7(4)
C(1)–Fe(1)–C(23)	97.2(2)	C(8)–N(1)–C(10)	115.7(4)	S(2)–C(12)–C(7)	118.8(4)
C(1)–Fe(1)–C(24)	96.6(2)	C(12)–N(2)–C(13)	117.7(4)	S(2)–C(17)–C(18)	120.1(4)
C(20)–Fe(1)–C(23)	96.8(2)	C(12)–N(2)–C(15)	123.6(4)		

Table 8
IR-data ^a, elemental analyses and mass data ^c of complexes **7**, **8**, **10**, **11**, **12**, **13**, **14** and **15**

Compound	IR: $\nu(\text{CO})$ and $\nu(\text{NH})$ (cm^{-1})	Elemental analyses (%)			M	λ_{max} (nm)
		C obs (calc.)	H obs (calc.)	N obs (calc.)		
7a	2037 (s), 1772 (s)	34.32 (34.41)	3.29 (3.21)	8.97 (8.92)	314 (314)	493, 614
7d	2049 (s), 1985 (s)	not analysed			372 (372)	463, 637
8a ^b	2061 (s), 2009 (vs), 1995 (sh), 1954 (m), 1942 (m) (4:1)	31.64 (31.74)	2.29 (2.22)	6.23 (6.17)	454 (454)	
8b	3313 (vw), 2078 (s), 2042 (vs), 2007 (vs), 2001 (sh), 1990 (m), 1959 (w), 1633 (m)	34.94 (34.73)	3.38 (3.33)	5.72 (5.79)	484 (484)	
8c	3315 (vw), 2080 (s), 2044 (vs), 2008 (vs), 1999 (sh), 1992 (m), 1961 (w), 1636 (m)				580 (580)	
8d	2071 (s), 2033 (vs), 2000 (vs), 1993 (vs), 1980 (m), 1951 (w)	37.46 (37.52)	4.91 (3.94)	5.43 (5.47)	512 (512)	
10a ^b	2095 (s), 2085 (m), 2045 (sh), 2040 (vs), 1959 (m), 1928 (s), 1712 (m)	36.49 (36.56)	2.65 (2.59)	4.41 (4.49)	624 (624)	
11a ^b	2063 (s), 2009 (vs), 1987 (m), 1966 (w), 1699 (m) (4:1)				568 (568)	
12d ^b	2035 (s), 1987 (s), 1709 (s) (4:1)	45.95 (45.86)	4.98 (5.14)	4.43 (4.48)	628 (628)	
13 ^b	1736 (m), 1719 (m)				316 (316)	
14	2062 (s), 2044 (s), 2024 (s), 2007 (m), 1984 (w)				484 (484)	
15	2084 (m), 2043 (s), 2007 (s)				344 (344)	

^a Measured in hexane, s = strong, m = medium, w = weak.

^b Measured in hexane/ CH_2Cl_2 (4:1).

^c Observed (calculated) FD masses of molecular ion M^+ (m/e); M^+ values are based upon ^{56}Fe isotope.

somewhat shorter than the corresponding Fe–C(sp^2) bonds in **10a** and **11a** and fall within the range normally found for Fe–C(sp^2) bonds [11,72–74]. As a result of the coupling reaction, the former alkyne triple bonds C(4)–C(7) and C(17)–C(20) are reduced to double bonds of 1.335(7) and 1.339(7) Å, respectively. The

central C(7)–C(12) single bond is oxidised to a double bond with a bond distance of 1.383(8) Å. This distance is rather long for a double bond. The N(1)–C(7) and the N(2)–C(12) bond distances of 1.365(7) and 1.385(6) Å, respectively, are rather short for C(sp^2)–N(sp^3) bonds and suggest partial double bond character for

these bonds. This is corroborated by the sum of the angles around N(1) and N(2) which are 356.8(7) and 356.9(7)°, respectively. All this may be explained by partial delocalisation in the N(1)–C(7)–C(12)–N(2) fragment. The S(1)–C(7), S(2)–C(12), S(1)–C(4) and S(2)–C(17) bonds distances are 1.786(6), 1.784(5), 1.774(5) and 1.805(6) Å, respectively. These bonds are somewhat longer than the mean value of 1.75 Å [75] for organic C(sp²)–S bonds, probably due to the co-ordination of sulfur to iron.

3.10. IR, UV–Vis spectroscopy and elemental analyses

The IR, UV–Vis and analytical data of complexes **7a,d**, **8a–d**, **9**, **10a**, **11a**, **12d**, **13**, **14** and **15** are listed in Table 8.

3.10.1. Complexes 7

The three terminal carbonyl ligands in **7a,d** give rise to two strong absorption bands in the terminal $\nu(\text{CO})$ region, a sharp band at higher frequency and a broad, slightly asymmetric absorption band at lower frequency. A similar pattern is observed for the (alkyl-DAB)M(CO)₃ (M = Fe, Ru) [31,76–78] complexes. The position of the CO stretching bands of **7a,d** compare well with those of Fe(CO)₃(p-Tol, p-An-DAB) [32], suggesting that the DTO ligands also possess a similar low-lying π^* -LUMO level. The higher CO stretching frequencies of **7d** compared to **7a** indicate that the Et₄-DTO is a better π -acceptor than *cyclo*-DTO. This agrees well with the position of the low energy absorption band of **7d** in the UV–Vis spectrum, which is found at lower energy than that of **7a**, indicating a lower π^* -level (see below).

The UV–Vis spectra of **7a,d** in hexane show a very intense absorption band at 616 and 637 nm, respectively. A second band of low intensity is located at 493 and 463 nm. The absorption bands at low energy show hardly any solvatochromic behaviour [**7a**; 616 nm (hexane), 623 nm (THF): **7b**; 637 nm (hexane), 641 nm (THF)]. The pattern of the bands in the UV–Vis spectra of complexes **7** resembles that found for Fe(CO)₃(R-DAB) [31,78] and Fe(CO)₃(α -iminoketone) [33], except that the low energy band is further redshifted by 80 to 120 nm. The absence of solvatochromism in Fe(CO)₃(R-DAB) and Fe(CO)₃(α -iminoketone) has been attributed, on basis of MO-calculations and resonance Raman spectra, to a strong mixing of the metal d _{π} -(HOMO) orbitals and the low lying α -diimine π^* -(LUMO) orbitals [31]. As a result, the transition between these orbitals mainly has metal–ligand bonding to anti-bonding character and hardly possesses any charge transfer character.

The presence of a similar transition in complexes **7a,d** as in Fe(CO)₃(R-DAB) and Fe(CO)₃(α -iminoketone) indicates that the DTO possess a similar delocalised π^* -orbital, however, of lower energy than those of

R-DAB and α -iminoketone, which is indicated by the low energy shift of the absorption bands. This further implies that the DTO ligand in **7a, d** is coordinated to iron in a σ -S, σ -S' chelate fashion and adopts a planar-*syn* conformation to achieve a maximum of orbital overlap with formation of a low lying π^* -orbital. This is confirmed by the ¹H and ¹³C NMR data (see Section 3.11). Analogous to Fe(CO)₃(R-DAB) and Fe(CO)₃(α -iminoketone), the bands at 493 and 463 nm for **7a,d** are assigned to a LF transition.

3.10.2. Complexes 8

The six terminal CO ligands in **8a** in hexane/CH₂Cl₂ (4:1) give rise to five IR absorption bands of medium to very strong intensity in the $\nu(\text{CO})$ region. The pattern and position of the CO stretching bands compare very well with those of the isostructural complexes Fe₂(CO)₆(L) (L = R-DAB, α -iminoketone and esters). When the IR is measured in CH₂Cl₂, three broad bands are observed at 2095, 2007 and 1950 cm⁻¹, with a shoulder at 1992 cm⁻¹.

The six terminal carbonyls in complexes **8b–d** give rise to six CO stretching bands. It must be noted that the weak absorption at the low frequency side of the spectrum has never been reported before. The pattern and the position of the five other medium to very strong CO stretching bands are characteristic for an Fe₂(CO)₆(μ_2 -S)₂ moiety [67,79,80]. The newly formed imine fragment in **8b,c** gives rise to an absorption band of medium intensity at 1633 and 1636 cm⁻¹, respectively. The remaining N–H bond in **8b,c** gives rise to a weak absorption in the $\nu(\text{N–H})$ region at 3313 and 3315 cm⁻¹. These absorptions are significantly shifted to higher frequency compared to those of the free ligands at 3154 cm⁻¹ (**b**) and 3174 cm⁻¹ (**c**) (KBr). The shift is due to the change from an “acidic” sp² hybridised nitrogen (free ligand) to a basic sp³ hybridised nitrogen in **8b,c**. In the ¹H NMR, a very pronounced shift is also observed for the N–H resonance.

3.10.3. Complexes 10a and 11a

The IR spectrum of **10a** in hexane/CH₂Cl₂ (4:1) shows six absorption bands in the terminal $\nu(\text{CO})$ region between 2095 and 1926 cm⁻¹. The two high frequency bands at 2095 and 2040 cm⁻¹ (broad) are assigned to the Fe(II)(CO)₃ centre of the bicyclo [2.2.1] structure. The broad band at 2040 cm⁻¹ is probably composed of two, nearly coincident, vibrations of the Fe(CO)₃ fragment and one band (see below) of the Fe(CO)₄ moiety. The position of the two bands of the Fe(II)(CO)₃ centre agrees quite well with those of the isostructural bicyclo[2.2.1]Fe(CO)₃ complex [11]. Consequently, the three absorptions at low frequency, 1964, 1939 and 1926 cm⁻¹, are assigned to the carbonyls of the axially S-coordinated Fe(CO)₄ fragment. The pattern of these bands compares well with that of axially

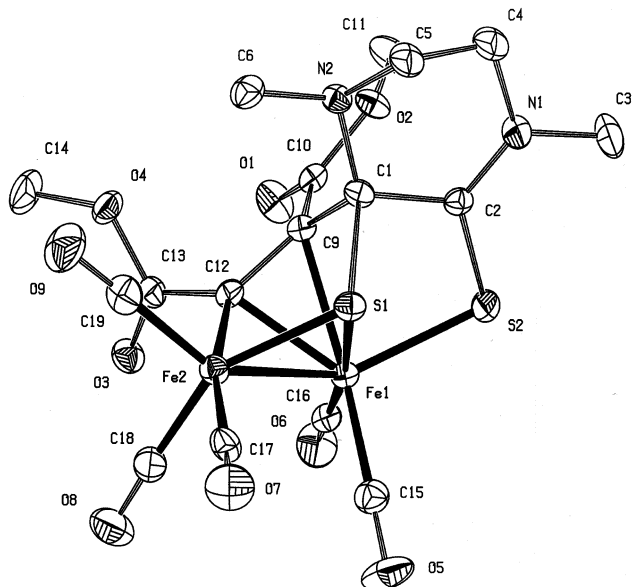


Fig. 8. ORTEP drawing (50% probability level) of the molecular structure of **11a**. Hydrogen atoms and solvent molecule are omitted for clarity.

coordinated $\text{Fe}(\text{CO})_4(\text{L})$ ($\text{L} = \text{PR}_3$) complexes [81]. The bands are positioned at somewhat lower frequency than those of $\text{Fe}(\text{CO})_4(\text{P}^n\text{Bu}_3)$ [81], showing that the sulfur in **10a** is a strong donor. For $\text{Fe}(\text{CO})_4(\text{P}^n\text{Bu}_3)$, an absorption band of medium intensity is also found at 2047 cm^{-1} . Therefore, the shoulder at 2045 cm^{-1} is assigned to the corresponding CO stretching band of the $\text{Fe}(\text{CO})_4$ fragment in **10a**. The carbonyl ester groups in **10a** give rise to an absorption at 1712 cm^{-1} .

The five terminal CO ligands in **11a** give rise to a characteristic absorption pattern for this type of com-

plex. The pattern is very similar to that of complexes A and B (cf. Fig. 8), although in complex A the σ, π -coordination of the alkene bond is opposite to that in **11a**. The absorption bands of **11a** are found at approximately 10 cm^{-1} to higher frequency compared to those in both A and B, which is probably due to the better electron donor properties of sulfur in **11a** compared to that of oxygen in A and B. The absorption at 1699 cm^{-1} is assigned to the carbonyl ester groups.

3.10.4. Complexes **12d** and **13**

The two terminal CO ligands in **12d** give rise to two strong absorption bands at 2035 and 1987 cm^{-1} . These absorptions lie at rather low frequency for a formal Fe(II) centre. This is probably due to the almost perfect *trans*-position of the S-donors and the carbonyl ligands in **12a** [cf. Fig. 9; $\text{S}(1)\text{-Fe}(1)\text{-C}(23) = 92.67(19)^\circ$, $\text{S}(2)\text{-Fe}(1)\text{-C}(24) = 94.56(19)^\circ$] which enhance π -back donation in this direction. The ester carbonyl groups give rise to an absorption at 1709 cm^{-1} . The ester carbonyl groups of the organic thiophene derivative **13** give rise to two absorptions in the organic carbonyl region at 1736 and 1719 cm^{-1} .

3.11. NMR spectroscopy

The ^1H and ^{13}C NMR spectroscopic data of complexes **7**, **8**, **10**, **11**, **12**, **13**, **14** and **15** are listed in Tables 9 and 10, respectively.

3.11.1. Complexes **7**

The ^1H NMR spectrum of the free $\text{Et}_4\text{-DTO}$ ligand shows a pair of equally intense ABX_3 patterns [14]. This means that the ethyl groups on each amide nitrogen are

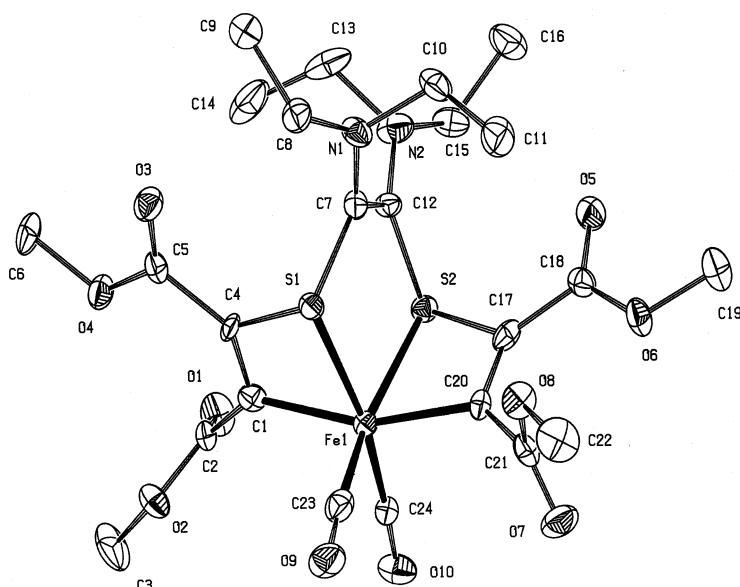


Fig. 9. ORTEP drawing (50% probability level) of the molecular structure of **12d**. Hydrogen atoms are omitted for clarity.

Table 9
¹H NMR data ^{a,b} of complexes **7**, **8**, **10**, **11**, **12**, **13**, **14** and **15**

Compound	δ -Values (ppm)
7a	3.41 (4H, s, 2 × NCH ₂), 3.21 (6H, s 2 × NCH ₃)
7d	3.52 (4 × 2H, q, 6.8Hz, NCH ₂ CH ₃), 1.07 (4 × 3H, t, 6,8Hz, NCH ₂ CH ₃)
8a	3.45 (1H, m, NCH), 3.33 (1H, m, NCH), 2.94 (1H, s, NCH ₃), 2.78 (3H, s, NCH ₃), 2.78 (1H, m, NCH)
8b	4.17 (1H, d, 6.0Hz, SCH), 4.17 (1H, sept, 6.2 Hz, C=NCH(CH ₃) ₂), 3.16 (1H, dsept, 6.2 Hz, 6.2 Hz, CNCH(CH ₃) ₂), 1.64 (1H, dd, 6.2 Hz, 6.0 Hz, NH), 1.22, 1.20 (2 × 3H, d, 6.3 Hz, CH(CH ₃)), 1.16, 1.10 (2 × 3H, d, 6.3 Hz, CH(CH ₃))
8c	7.35 (10H, m, arylH), 4.95 (2H, s, C=NCH ₂), 4.20 (1H, d, 4.9Hz, SCH), 4.16 (dd, 13.7Hz, 7.0Hz, CNCH), 3.97 (dd, 13.7Hz, 6.4Hz, CNCH), 2.35 (ddd, 7.0Hz, 6.4Hz, 4.9Hz, NH)
8d	2.88 (4 × 2H, q, 7.1 Hz, NCH ₂ CH ₃), 0.98 (4 × 3H, t, 7.1 Hz, NCH ₂ CH ₃)
10a	4.02 (1H, ddd, 12.6 Hz, 9.1Hz, 4.0 Hz, NCH), 3.84 (1H, ddd, 12.6 Hz, 9.1 Hz, 4.0 Hz, NCH), 3.81 (3H, s, OCH ₃), 3.70 (3H, s, OCH ₃), 3.65 (3H, br., s, NCH ₃), 3.60 (1H, ddd, 12.3 Hz, 4.0 Hz, 4.0 Hz, NCH), 3.18 (1H, ddd, 12.3 Hz, 4.0 Hz, 4.0 Hz, NCH), 2.73 (3H, s, NCH ₃)
11a	3.84 (3H, s, OCH ₃), 3.80 (1H, ddd, 10.7 Hz, 3.6 Hz, 2.5 Hz, NCH), 3.65 (3H, s, OCH ₃), 3.52 (3H, br, s, NCH ₃), 3.29 (1H, ddd, 10.7 Hz, 3.6 Hz, 2.5 Hz, NCH), 2.69 (2H, m, 2 × NCH), 2.28 (3H, s, NCH ₃)
12d	3.74 (3H, s, OCH ₃), 3.65 (4H, dq, 14.0 Hz, 7.0 Hz, 4 × NCH), 3.61 (3H, s, OCH ₃), 3.46 (4H, dq, 14.0 Hz, 7.0 Hz, 4 × NCH), 1.02 (12H, t, 7.0 Hz, 4 × NCH ₂ CH ₃)
13	3.92 (12H, s, 4 × OCH ₃)

^a The resonances are characterised in consecutive order by δ -value (in ppm, relative to Me₄Si), rel. intensity, multiplicity, coupling constant and assignment.

^b Measured in CDCl₃ at 293 K and 300.13 MHz; s = singlet, d = doublet, t = triplet, q = quartet, dd = double doublet, dq = double quartet, sept = septet, dsept = double septet, ddd = double double doublet.

inequivalent due to the hindered rotation around the C–N axis as a result of the electron delocalisation within the thioamide N–C–S moieties (cf. Fig. 1). Furthermore, the methylene protons in each ethyl group are diastereotopic. This means that the N–C=S planes are tilted relative to each other in solution and that the barriers for rotation around the chiral C–C axis are high in solution. In the *S,S'*-chelate complex PtCl₂(Et₄-DTO) [14], an ABX₃ pattern is also observed, indicating that the chiral axis is still present. In Re(CO)₃Br(Et₄-DTO) [21], the ethyl groups are again inequivalent and give rise to a complicated pattern of resonances.

As opposed to the free ligand and the above-mentioned complexes, the ¹H and ¹³C spectra of complex **7d** show 4 equiv. ethyl groups, i.e. one quartet and one triplet, indicating that in this case the S–C–C–S fragment is flat, and rotation around the C–N bond is not hindered on the NMR time scale. Analogously, in Mo(CO)₂(PR₃)₂(Me₄-DTO) [18,19] the four methyl groups give rise to one singlet while in Mo(CO)₄–*n*(PR₃)_{*n*}(Me₄-DTO) (*n* = 0, 1) the methyl groups are pairwise inequivalent and give rise to two resonances of equal intensity. The equivalency of the methyl groups is attributed to the formation of a flat S–C–C–S backbone due to extensive π -back donation from the electron rich Mo(CO)₂(PR₃)₂ into the π^* -orbital of the Me₄-DTO ligand. Consequently, the conjugation within the thioamide moieties is lost and the rotation around the C–N bond becomes significantly less hindered, which results in equivalent methyl groups. Accordingly, on this basis we propose that the DTO ligands in **7a,d** are coordinated in a planar-syn σ -S, σ -S' chelate fashion,

which agrees well with the IR and UV–Vis data. As a result of the extensive π -back donation, the thiocarbonyl carbon atom resonances are shifted 22.7 and 19.4 ppm to lower frequency in comparison with those of the free ligands. Comparable shifts to lower frequency have been observed for the ketone carbon atom in Fe(CO)₃(α -iminoketone) [33], whereas somewhat smaller shifts have been found for the imine carbon atoms in Fe(CO)₃(R-DAB) [32] and Fe(CO)₃(α -iminoketone). The three terminal CO ligands in complexes **7a,d** give rise to a single resonance at 213.6 and 210.8 ppm indicating that they rapidly interchange on the NMR time scale at 263 K. This interchange has also been observed for the M(CO)₃(R-DAB) (M = Fe, Ru) [76,82,83] and Fe(CO)₃(α -iminoketone) and may be explained by Berry pseudo-rotations [84].

3.11.2. Complexes **8**

In the ¹³C NMR spectrum of **8a** the σ -S coordinated thiocarbonyl carbon atom resonates at 194.0 ppm, a shift of 7.1 ppm to higher frequency compared to the free ligand. The η^2 -C=S coordinated thiocarbonyl carbon atom resonance, observed at 95.7 ppm, is shifted 91.4 ppm to lower frequency. These shifts are typical for a σ -S, μ_2 -S, η^2 -C=S co-ordination of the DTO ligand and have also been observed for the isostructural complexes M₂(CO)₆(L) (Fe, Ru, Os; L = R-DAB, α -imino-ketone and ester) [33,52,53,55,85].

Since the *cyclo*-DTO ligand in Fe₂(CO)₆(*cyclo*-DTO) is asymmetrically coordinated, the six terminal carbonyl ligands in **8a** are inequivalent. In a rigid skeleton this should give rise to six independent resonances for the carbonyl groups. At 263 K, three sharp resonances are

observed of equal intensity, while at room temperature a fourth resonance is observed which does not lie at the weighted average ppm value of the three signals at 263 K. This is indicative for local scrambling of the carbonyl groups on one iron centre at 263 K, while the carbonyl groups on the other iron centre are in the limit of slow exchange. The same dynamic behaviour has been found for $\text{Fe}_2(\text{CO})_6(\alpha\text{-iminoester})$ [55]. Like in the $\text{Fe}_2(\text{CO})_6(\alpha\text{-iminoester})$ complexes, the three separate CO resonances observed at 263 K correspond to the $\sigma\text{-S}'$, $\eta^2\text{-S}$ coordinated $\text{Fe}(\text{CO})_3$ centre and the single resonance, observed at room temperature, belongs to the $\mu_2\text{-S}$, $\eta^2\text{-C=S}$ coordinated $\text{Fe}(\text{CO})_3$ fragment.

Table 10
 ^{13}C NMR data ^a of complexes **7**, **8**, **10**, **11**, **12**, **13**, **14** and **15**

Compound	δ -Values (ppm)
7a	213.6 (3 \times CO), 164.4 (S=CN), 49.8 (NCH ₂), 43.0 (NCH ₃)
7d	210.8 (3 \times CO), 173.6 (S=CN), 46.9 (4 \times NCH ₂ CH ₃), 12.7 (4 \times NCH ₂ CH ₃)
8a	214.8, 210.2, 205.8 (3 \times CO), (214.1 3 \times CO) ^b , 194.0 (C=S), 95.7 (C-S), 52.1 (NCH ₃), 49.6 (NCH ₃), 44.1 (NCH ₂), 41.9 (NCH ₂)
8b ^c	209.2, 209.1, 208.9, 208.8, 206.7, 206.0 (6 \times CO), 162.1 (C=N), 67.4 (S-C), 58.0 (C-NCH(CH ₃) ₂), 47.7 (C=NCH(CH ₃) ₂), 23.9, 23.6, 23.4, 21.2 (4 \times CHCH ₃)
8c ^c	209.2, 209.1, 209.0, 208.8, 205.8, 205.5 (6 \times CO), 166.4 (C=N), 138.5, 138.0 (2 \times <i>i</i> -arylC), 129.1, 129.1, 128.8, 128.5 (4 \times <i>o</i> / <i>m</i> -arylC), 128.0, 127.9 (2 \times <i>p</i> -arylC), 68.3 (S-C), 60.4 (NCH ₂), 51.5 (NCH ₂)
8d	209.4 (2 \times CO), 208.7 (2 \times CO), 208.7 (2 \times CO), 141.8 (2 \times C=C), 47.1 (4 \times NCH ₂), 14.6 (4 \times NCH ₂ CH ₃)
10a	215.4 (4 \times CO), 204.5, 203.9, 203.3 (3 \times CO), 198.0 (Fe-C _{α} =C), 180.8 (S=C), 175.0, 164.5 (2 \times C=O), 142.8 (Fe-C=C _{β}), 94.5 (S-C), 53.4 (NCH ₂), 53.1, 52.8 (2 \times OCH ₃), 47.3 (NCH ₃), 45.0 (NCH ₂), 40.1 (NCH ₃)
11b	213.3, 211.2 (2 \times CO), 208.6 (3 \times CO), 203.4 (Fe-C _{α} =C), 188.9 (C=S), 176.5, 168.5 (2 \times C=O), 99.5 (Fe-C=C _{β}), 93.0 (S-C), 53.0 (NCH ₂), 52.9, 52.8 (2 \times OCH ₃), 44.5 (NCH ₂), 43.2 (NCH ₃), 42.7 (NCH ₃)
12d	213.9 (2 \times CO), 193.2 (2 \times Fe-C _{α} =C), 173.8 (2 \times C=O), 156.8 (2 \times C=O), 128.0 (2 \times Fe-C=C _{β}), 127.7 (2 \times C=C), 53.2 (2 \times OCH ₃), 52.4 (2 \times OCH ₃), 46.2 (2 \times NCH ₂), 14.3 (2 \times NCH ₂ CH ₃)
13	163.3 (2 \times C=O), 160.8 (2 \times C=O), 137.5 (2 \times C=C), 136.0 (2 \times C=C), 54.0 (2 \times OCH ₃), 53.9 (2 \times OCH ₃)
14	209.6 (9 \times CO)
15	209.0 (6 \times CO)

^a The resonances are characterised in consecutive order by δ -value (in ppm, relative to Me₄Si), and assignment, measured in CDCl₃ at 263 K and 75.47 MHz.

^b Measured at 293 K.

^c Measured at 203 K.

In complexes **8b–c** one of the amide proton atoms is 1,3-H shifted to the central carbon atom of the other thioamide fragment. The remaining N–H proton in **8b** gives rise to a double doublet at 1.64 ppm due to the coupling with the new C–H proton and the ¹PrC–H proton. In **8c** it gives rise to a double double doublet at 2.54 ppm due to the coupling with the new C–H proton and the two diastereotopic methylene protons of the benzyl substituent. Compared to the free ligands (10.22 ppm (**b**), 10.53 ppm (**c**)), the N–H resonances are shifted drastically to lower frequency due to the change from a delocalised (R)H–N(sp²)–C–S moiety to a (R)H–N(sp³)–C–S moiety. The reduced thiocarbonyl carbon atom in **8b,c** is chiral. As a result the methylene protons of the benzyl substituent in **8c** attached to the amide nitrogen are diastereotopic and are observed as double doublets at 4.16 and 3.97 ppm due to the coupling with the N–H proton and a geminal coupling of 13.7 Hz. The methylene protons of the benzyl on the imine nitrogen are observed as a singlet at 4.95 ppm. The reduced thiocarbonyl carbon atom in **8b,c**, observed at 67.4 and 68.7 ppm, respectively, is strongly shifted to a lower frequency compared to the corresponding carbon atom in the free ligand due to the rehybridisation from sp² to sp³. The newly formed imine carbon atoms resonate at 162.1 and 166.4 ppm, normal ppm values for imine carbon atoms.

As in complex **8a**, the DTO ligand in **8b–c** is asymmetrically coordinated, which should, in a rigid skeleton, result in six independent resonances for the six carbonyl ligands. At 323 K, two closely spaced resonances of equal intensity are observed. Upon cooling to room temperature one broad resonance is observed which disappears in the baseline at 263 K. Further cooling to 203 K results in six sharp resonances for the six terminal carbonyl ligands. This means that at 323 K the carbonyl ligands on both the Fe(CO)₃ fragments are in the limit of fast exchange, while at 203 K both the Fe(CO)₃ fragments are in the limit of slow exchange. Individual assignment, however, is not possible.

As expected, the symmetrical complex **8d** shows only one set of resonances in the ¹H and ¹³C NMR spectra for all corresponding nuclei in the two molecular halves, even down to 163 K (freon/CH₂Cl₂). The four ethyl groups give rise to one quartet and one triplet indicating that the rotation around the C–N bond is not hindered even at very low temperatures. Obviously, the partial double bond character in one of the N–C bonds which was found in the solid state structure of **8d** is not present in solution. The carbon atoms of the central C=C bond resonate at 141.8 ppm, a normal ppm value for alkene carbon atoms. The two equal Fe(CO)₃ fragments should in a rigid structure give rise to three Fe-carbonyl resonances. This was indeed observed at 203 K. Upon heating the NMR sample the signals broaden and disappear in the baseline at 243 K and

further heating to room temperature results in one sharp resonance at 209.1 ppm. This means that at room temperature the three carbonyl ligands on each $\text{Fe}(\text{CO})_3$ fragment are in the limit of fast exchange and they are in the limit of slow exchange at 263 K.

3.11.3. Complexes **10a** and **11a**

In the ^1H NMR spectrum of **10a** all four protons of the $\text{NCH}_2\text{CH}_2\text{N}$ moiety are inequivalent, giving rise to four double double doublets. As a result of the cycloaddition reaction the protons of the two ester methyl groups of DMAD are inequivalent and resonate at 3.81 and 3.70 ppm. The ^{13}C NMR spectrum shows the characteristic resonances for a [2.2.1] bicyclic structure. The former thiocarbonyl bridgehead carbon atom resonance is shifted 70.2 ppm to lower frequency compared to **7a** due to the rehybridisation of this carbon from sp^2 to sp^3 . The intact thiocarbonyl carbon atom, observed at 180.8 ppm, is shifted 16.4 ppm to higher frequency indicating the decrease of π -back donation to this isolated thiocarbonyl fragment. The two former alkyne carbon atoms resonate at significantly different ppm values. The former alkyne carbon C_β , which is C–C connected to the bridgehead carbon atom, resonates at 142.8 ppm. The position of this resonance compares well with that of the corresponding carbon atom in the isostructural [2.2.1] complex **6** (cf. Scheme 1). The C_α carbon atom, σ -bonded to iron, resonates at 198.0 ppm which compares well with the resonances of the corresponding $\text{Fe}-\text{C}(\text{sp}^2)$ carbons atoms in [2.2.1] [11,69] and [2.2.2] [4,86,87] bicyclic complexes. The additional shift of 56 ppm to higher frequency is due to paramagnetic shielding of the iron centre. The three terminal CO ligands on the [2.2.1] $\text{Fe}(\text{CO})_3$ centre give rise to three resonances at 204.5, 203.9 and 203.3 ppm. The four CO ligands on the $\text{Fe}(\text{CO})_4$ fragment appear as one signal at 215.4 ppm, indicating that they rapidly interchange on the NMR time scale.

The ^1H and ^{13}C NMR spectra of complex **11a** show many similarities with that of **10a** except for the C_β alkene carbon atom. The σ -bonded C_α alkene carbon in **11a** resonates at 203.4 ppm, which is comparable with the resonance at 198.0 ppm in **10a** and somewhat to higher frequency compared to those at approximately 189.0 ppm in A and B, respectively. The C_β alkene carbon atom resonates at 93.0 ppm, which compares quite well with the resonance at 98.0 ppm of the corresponding carbon atom in B. In complex A C_β is found at approximately 77 ppm, a shift of 16 ppm to lower frequency, which is probably due to the change in σ,π -co-ordination of the alkene. The terminal carbonyl ligands give rise to three resonances with relative intensities of 1:1:3 going from high to low frequency. Apparently, the carbonyls on the $\text{Fe}(\text{CO})_2$ fragment are in the limit of slow exchange and the carbonyls on the

$\text{Fe}(\text{CO})_3$ fragment are in the limit of fast exchange, at 263 K.

3.11.4. Complex **12d** and compound **13**

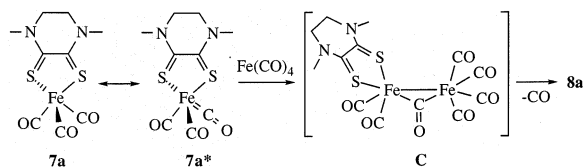
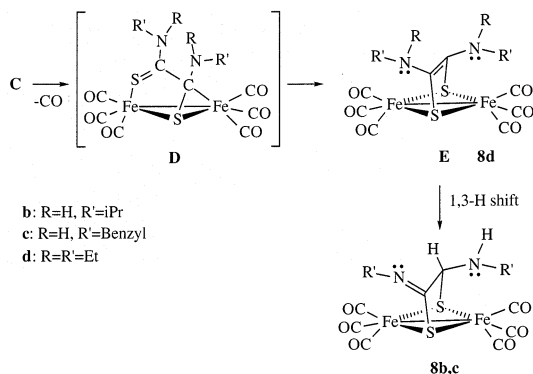
The ^1H and ^{13}C NMR spectra of complex **12d** show only one set of resonances for the two structurally similar halves of the molecule. However, from the solid state structure it could be seen that **12d** is not symmetric since the two four-membered rings are almost perpendicular. This means that in solution the molecule is involved in a dynamic process by which the two molecular halves of the molecule become equivalent. As opposed to complexes **7d** and **8d**, the methylene protons of the 4 equiv. ethyl groups in **12d** are diastereotopic due to the chiral sulfur atoms and give rise to two double quartets at 3.65 and 3.46 ppm, with a geminal coupling of 14.0 Hz. The methyl groups give rise to a triplet at 1.02 ppm. The partial delocalisation within the $(\text{Et}_2)\text{N}-\text{C}=\text{C}-\text{N}(\text{Et}_2)$ fragment, which is suggested by the bond lengths in the solid state structure of **12d**, apparently does not hinder a free rotation around the C–N bond in solution. This makes the two ethyl groups on each NEt_2 group equivalent. Further, a flip-flop exchange of the axial and equatorial sulfur atoms exchanges the two NEt_2 groups and also all other nuclei. The carbon atoms of the central C=C bond resonate at 127.7 ppm, a normal position for a $\text{C}(\text{sp}^2)$ resonance. The C_α alkene carbon atoms, σ -bonded to iron, resonate at 193.3 ppm. This is a normal ppm value for an $\text{Fe}-\text{C}(\text{sp}^2)$ [9,11,72–74] carbon atom and comparable with that of 198.0 ppm in **10a**. The C_β alkene carbon atom is observed at 128.0 ppm, which is within the range generally observed for sp^2 -alkene carbon atoms.

Surprisingly, the protons of the four carboxy methyl groups in **13** give rise to one singlet in the ^1H NMR. However, in the ^{13}C NMR two sets of resonances are observed for the ester methyl carbon atoms and the carbonyl carbon atoms. Obviously, the resonances of the pairwise inequivalent carboxy methyl protons coincide by chance and thus appear as one singlet. The alkene carbon resonances at 137.5 and 136.0 ppm compare well with those of thiophene-2-aldehyde and thiophene-3-aldehyde [88]. The ester carbonyl carbon resonances are found in the expected region at 163.3 and 160.8 ppm.

3.12. Complex formation

3.12.1. Formation of complexes **7**

The reaction of $\text{Fe}_2(\text{CO})_9$ with the DTO ligands **a–d** at room temperature in THF or toluene results in initial formation of the deep blue–green $\text{Fe}(\text{CO})_3(\text{DTO})$ complexes (**7**), probably via a monodentate σ -S coordinated $\text{Fe}(\text{CO})_4[\text{S}=\text{C}(\text{NRR}')-\text{C}(\text{NRR}')=\text{S}]$ intermediate. This type of complexes' monodentate has been isolated for

Scheme 5. Proposed reaction mechanism for the formation of **8a**.Scheme 6. Proposed reaction mechanism for the formation of **8b–d**.

thioureas and amides [37]. Unfortunately however, complexes **7** can only be isolated with ligands **a** and **d**, because with these ligands the further reaction with $[\text{Fe}(\text{CO})_4]$, resulting in the dinuclear complexes **8a,d**, is relatively slow. Complexes **7b,c** react very fast with $[\text{Fe}(\text{CO})_4]$ to the corresponding dinuclear complexes **8b,c**. Analogous to $\text{Fe}(\text{CO})_3(\text{L})$ ($\text{L} = \text{R-DAB}$, α -iminoketone) and $\text{Mo}(\text{CO})_2(\text{PR}_3)_2(\text{DTO})$ [19] ($\text{R} = \text{alkyl}$), complexes **7a,d** are intensely coloured and extremely air-sensitive. The stoichiometry of **7a** has been established by elemental analysis. Complexes **7a,d** are well soluble and stable in common solvents such as hexane (**7d**), Et_2O , toluene, and THF, but decompose in chlorinated solvents like CHCl_3 , as is the case for $\text{Fe}(\text{CO})_3(\text{L})$ ($\text{L} = \text{R-DAB}$, α -iminoketone).

3.12.2. Formation of $\text{Fe}_2(\text{CO})_6(\text{cyclo-DTO})$ (**8a**)

Reaction of $\text{Fe}(\text{CO})_3(\text{cyclo-DTO})$ (**7a**) with $[\text{Fe}(\text{CO})_4]$ in THF or toluene results in the formation of the known type of dinuclear complex $\text{Fe}_2(\text{CO})_6(\text{cyclo-DTO})$ (**8a**), in which the *cyclo-DTO* ligand is σ -S, μ_2 -S', η^2 -C=S coordinated to the metal centres. Complex **8a** is probably formed via the dinuclear CO-bridged intermediate C (cf. Scheme 5), since similar intermediates have been proposed for the formation of the isostructural complexes $\text{Fe}_2(\text{CO})_6(\text{R-DAB})$ [89], $\text{Fe}_2(\text{CO})_6(\alpha\text{-iminoketone})$ [33] and $\text{Fe}_2(\text{CO})_6(\alpha\text{-iminoester})$ [55]. The formation of C can be described as an isolobal analogue [90,91] of the addition of a carbene to an olefin giving a cyclopropane ring system. In this case $[\text{Fe}(\text{CO})_4]$ is isolobal with a carbene and adds to the $\text{Fe}=\text{C}$ double bond (isolobal with an olefin) in resonance structure **7a*** with formation of intermediate C.

Subsequent π -co-ordination of one C=S bond (μ_2 -S, η^2 -C=S co-ordination) with concomitant extrusion of CO completes the structure of **8a**. Complex **8a** is isolated as a dark-brown air-sensitive powder. In crystalline form it is slightly air-sensitive. In THF, complex **8a** is formed in good yield (70%) and in toluene in moderate yield (35%). Obviously, in toluene also other reaction pathways play a role, which is expressed by the formation of the new dinuclear complex **9a**, although it is formed in very low yield.

3.12.3. Reaction of **8a** with CO

Treatment of $\text{Fe}_2(\text{CO})_6(\text{R-DAB})$ with carbon monoxide (40–50 bar) at elevated temperatures yielded the monomeric complexes $\text{Fe}(\text{CO})_3(\text{R-DAB})$ and $\text{Fe}(\text{CO})_5$. Reaction of $\text{Fe}_2(\text{CO})_6(\text{cyclo-DTO})$ (**8a**) with CO, however, leads only to decomposition and the monomeric complex **7a** is not detected.

3.12.4. Formation of

$\text{Fe}_2(\text{CO})_6[\text{iPrN}=\text{C}(\text{S})-\text{S}(\text{C}(\text{H})\text{N}(\text{H})\text{iPr})]$ (**8b–c**) and $\text{Fe}_2(\text{CO})_6[\text{Et}(\text{Et})_2\text{N}-\text{C}(\text{S})=\text{S}(\text{C}-\text{N}(\text{Et})_2)]$ (**8d**)

Like complex **8a**, complexes **8b–d** are formed by initial reaction of the mononuclear $\text{Fe}(\text{CO})_3(\text{DTO})$ complexes **7b–d** with $[\text{Fe}(\text{CO})_4]$ resulting in the corresponding intermediates C. Subsequent π -co-ordination of one of the C=S bonds with concomitant extrusion of CO results in the formation of structure D, analogous to the formation of **8a** in Scheme 5. However, contrary to **8a**, structure D is not stable with ligands **b–d** and reacts further to form the final products **8b–d** which contain an $\text{Fe}_2(\text{CO})_6(\mu_2\text{-S})_2$ skeleton, i.e. the two sulfur atoms are reduced to sulfido groups. A possible mechanism for their formation is shown in Scheme 6. The next step in the reaction is probably initial π -co-ordination of the remaining thiocarbonyl C=S bond with concomitant redistribution of the electrons resulting in structure E, in which both sulfur atoms are reduced to sulfido groups and the central C–C bond is oxidised to a double bond. In the case of ligand **d** ($\text{R} = \text{R}' = \text{Et}$), structure E is stable and thus the final product (**8d**). However, in the case of ligands **b** ($\text{R} = \text{H}$, $\text{R}' = \text{iPr}$) and ligand **c** ($\text{R} = \text{H}$, $\text{R}' = \text{benzyl}$) one of the amide protons undergoes a subsequent 1,3-H shift to the thiocarbonyl carbon atom of the other thioamide moiety resulting in the final products **8b, c**. Cleavage of the N–H bond is often observed in reactions of R_2 -DTO ligands with metal ions giving rubeanate-DTO complexes [14,20]. In those cases, however, the proton is lost from the complex, e.g. the reaction of *cis*- $[\text{PtL}_2\text{R}_2]$ with $\text{H}_2\text{-R}'_2\text{-DTO}$ results in $[\text{PtL}(\text{R})(\text{H-R}'_2\text{-DTO})] + \text{L} + \text{RH}$.

The observation that **8a** is stable and does not react further to form an $\text{Fe}_2(\text{CO})_6(\mu_2\text{-S})_2$ skeleton, even upon heating to 70 °C in toluene, is probably due to the reduced flexibility of the cyclic DTO ligand, which

apparently prevents π -co-ordination of the second C=S bond.

3.12.5. Formation of **10a**

The formation of complex **10a** is shown in Scheme 3. In the earlier parts of this series we have demonstrated the isolobal analogy between the M–N=C fragment in $M(\text{CO})_n(\text{CNR})_{3-n}(\text{R}^1\text{-DAB})$ [$M = \text{Fe}, \text{Ru}$] and an azomethine ylide, and the isolobal analogy between the Fe–O=C fragment in $\text{Fe}(\text{CO})_{3-n}(\text{PR}_3)_n(\alpha\text{-iminoketone})$ and a carbonyl ylide, which are both well known organic 1,3-dipoles. Likewise, the Fe–S=C fragment in $\text{Fe}(\text{CO})_3(\text{DTO})$ is isolobally related to a thiocarbonyl ylide which is also a known organic 1,3-dipole [92].

On this basis, the in situ reaction of **7a** with the activated alkyne DMAD is described as an oxidative 1,3-dipolar cycloaddition across the Fe–S=C fragment, resulting in the stable bicyclo[2.2.1] complex **10a** (cf. Scheme 3). In **10a** an additional $\text{Fe}(\text{CO})_4$ fragment is coordinated to the sulfido sulfur of the cycloadduced Fe–S=C fragment. In the reaction of pure **7a** with DMAD, **10a** is also formed, however, in only 5% yield. The $\text{Fe}(\text{CO})_4$ fragment is supplied by partial decomposition. This strongly suggests that the coordinated $\text{Fe}(\text{CO})_4$ fragment is essential, and stabilises the [2.2.1] bicyclic structure probably by preventing insertion of CO into the Fe–S bond which would normally be the next step in the reaction sequence. When insertion of CO in the Fe–S is possible, as in the case of reaction of pure **7a** with DMAD, mainly decomposition is observed. Apparently, the [2.2.2] bicyclic complex, which is formed after insertion of CO, or another intermediate

along the reaction co-ordinate, is unstable and decomposes.

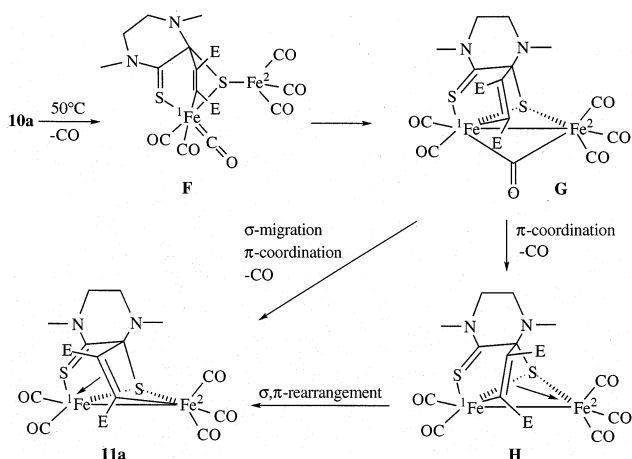
3.12.6. Formation of **11a**

Complex **11a** is formed on heating a toluene solution of **10a** to 50 °C. Since complex **11a** is similar to complex A, although the co-ordination of the alkene fragment is opposite, they are probably formed via a comparable reaction mechanism (cf. Scheme 7).

Like the formation of intermediate A, the formation of intermediate G can be seen as an isolobal analogue to the reaction of a carbene to an olefin. In the case of **10a**, dissociation of one of the terminal CO ligands of the $\text{Fe}(\text{CO})_4$ fragment results in a $(\sigma\text{-S})\text{Fe}^2(\text{CO})_3$ fragment (isolobal with $[\text{Fe}(\text{CO})_4]$), which is isolobal with a carbene. Subsequent intramolecular addition of this carbene to the Fe=C bond of one of the three terminal CO ligands on Fe^1 leads to intermediate G. The next step may be either (i) π -co-ordination of the alkene to Fe^2 with concomitant extrusion of CO leading to intermediate H which in turn isomerises via a σ, π -rearrangement to the final product **11a**, or (ii) first σ -migration, i.e. breakage of the Fe¹–C σ -bond and formation of a new σ -bond to Fe^2 , followed by π -co-ordination of the alkene to Fe^1 with concomitant loss of CO. The change in co-ordination of the alkene is probably due to the reduced flexibility of the cyclic DTO ligand, which makes the observed co-ordination apparently thermodynamically more favourable.

3.12.7. Formation of **12d**

From the structure of complex **12d** it is clear that it is not formed via a 1,3-dipolar cycloaddition reaction. This may be due to the bulky $\text{N}(\text{Et})_2$ groups which hinder attack at the thiocarbonyl carbon atom. The formation of **12d** may be rationalised by two successive insertions of DMAD into Fe–S σ -bonds, with recoordination of the oxidised sulfur atoms to iron by σ -donative bonds. It is, however, difficult to propose a mechanism for the formation of **12d** and **13** because no intermediates can be observed. It seems however likely that a “dithiolate” type of complex plays a role in the formation of complex **12d** (cf. Fig. 10). Due to the extensive π -back donation of iron into the low lying $\pi^*\text{-LUMO}$ of the $\text{Et}_4\text{-DTO}$ ligand, **7d** can be considered to have a (dithiolate)Fe(II) resonance structure with an open co-ordination site. Co-ordination of the alkyne DMAD to the open co-ordination site and subsequent insertion in the Fe–S bond, followed by loss of CO and a second insertion of DMAD, would give **12d**.



Scheme 7. Proposed reaction mechanism for the formation of **11a**.

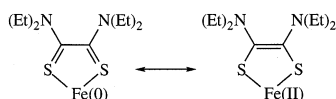


Fig. 10. Two resonance structures for Fe(DTO) complexes.

Acknowledgements

The investigation was in part supported (A.L.S., N.V.) by the Netherlands Foundation for Chemical

Research (SON) with financial aid from the Netherlands Organisation for Scientific Research (NWO).

References

- [1] N. Feiken, H.-W. Frühauf, K. Vrieze, J. Fraanje, K. Goubitz, *Organometallics* 13 (1994) 2825.
- [2] H.-W. Frühauf, F. Seils, R.J. Goddard, M.J. Romao, *Angew. Chem., Int. Ed. Engl.* 22 (1983) 992; *Angew. Chem.* 95 (1983) 1014; *Angew. Chem., Suppl.* (1983) 1435.
- [3] H.-W. Frühauf, F.J. Seils, *J. Organomet. Chem.* 323 (1987) 67.
- [4] P.P.M. de Lange, H.-W. Frühauf, M. van Wijnkoop, M.J.A. Kraakman, M. Kranenburg, A.H.J.P. Groot, J. Fraanje, Y. Wang, M. Numan, *Organometallics* 12 (1993) 417.
- [5] P.P.M. de Lange, M. van Wijnkoop, H.-W. Frühauf, K. Vrieze, K. Goubitz, *Organometallics* 12 (1993) 428.
- [6] P.P.M. de Lange, R.P. de Boer, M. van Wijnkoop, J.M. Ernsting, H.-W. Frühauf, K. Vrieze, W.J.J. Smeets, A.L. Spek, K. Goubitz, *Organometallics* 12 (1993) 440.
- [7] M. van Wijnkoop, P.P.M. de Lange, H.-W. Frühauf, K. Vrieze, Y. Wang, K. Goubitz, C.H. Stam, *Organometallics* 11 (1992) 3607.
- [8] M. van Wijnkoop, P.P.M. de Lange, H.-W. Frühauf, K. Vrieze, W.J.J. Smeets, A.L. Spek, *Organometallics* 14 (1995) 4781.
- [9] M. van Wijnkoop, R. Siebenlist, J.M. Ernsting, P.P.M. de Lange, H.-W. Frühauf, E. Horn, A.L. Spek, *J. Organomet. Chem.* 482 (1994) 99.
- [10] M. van Wijnkoop, R. Siebenlist, P.P.M. de Lange, H.-W. Frühauf, K. Vrieze, W.J.J. Smeets, A.L. Spek, *Organometallics* 12 (1993) 4172.
- [11] R. Siebenlist, H.-W. Frühauf, K. Vrieze, W.J.J. Smeets, A.L. Spek, in press.
- [12] M.G.B. Drew, J.M. Kisenyi, G.R.J.C.S. Willey, *J. Chem. Soc., Dalton Trans.* (1982) 1729.
- [13] M.G.B. Drew, J.M. Kisenyi, G.R. Willey, S.O. Wandiga, *J. Chem. Soc., Dalton Trans.* (1984) 1717.
- [14] S. Lanza, G. Bruno, L.M. Scolaro, F. Nicolo, G.T.A. Rosace, *Tetrahedron Asymm.* 4 (1993) 2311.
- [15] M.G.B. Drew, J.M. Kisenyi, G.R.J.C.S. Willey, *Dalton Trans.* (1982) 1729; *J. Chem. Soc., Dalton Trans.* (1984) 1723.
- [16] L. Antolini, A.C. Fabretti, G. Franchi, L. Menabue, G.C. Pellacani, *J. Chem. Soc., Dalton Trans.* (1987) 1921.
- [17] S. Lanza, L.M. Scolaro, G. Rosace, *Inorg. Chim. Acta* 227 (1994) 63.
- [18] H. tom Dieck, M. Form, *Angew. Chem.* 87 (1975) 245; *Angew. Chem., Int. Ed. Engl.* 14 (1975) 250.
- [19] H. tom Dieck, M. Form, *Z. Anorg. Allg. Chem.* 515 (1984) 19.
- [20] G. Rosace, G. Bruno, L.M. Scolaro, F. Nicolo, S. Sergi, S. Lanza, *Inorg. Chim. Acta* 208 (1993) 59.
- [21] P.C. Servaas, D.J. Stufkens, A. Oskam, P. Vernooijs, E.J. Baerands, D.J.A. De Ridder, C.H. Stam, *Inorg. Chem.* 28 (1989) 4194.
- [22] R. Sustmann, *Tetrahedron Lett.* (1971) 2721.
- [23] R. Sustmann, H. Trill, *Angew. Chem., Int. Ed. Engl.* 11 (1972) 838.
- [24] R. Sustmann, *Pure Appl. Chem.* 40 (1974) 569.
- [25] K.N. Houk, K. Yamaguchi, *1,3-Dipolar Cycloaddition Chemistry*, Wiley, New York, 1984, p. 407 chapter 13.
- [26] W.C. Herdon, *Chem. Rev.* 72 (1972) 157.
- [27] K. Fukui, *Acc. Chem. Res.* 4 (1971) 57.
- [28] L.H. Polm, C.J. Elsevier, G. van Koten, J.M. Ernsting, D.J. Stufkens, K. Vrieze, R.R. Andréa, C.H. Stam, *Organometallics* 6 (1987) 1096.
- [29] N. Feiken, H.-W. Frühauf, K. Vrieze, N. Veldman, A.L. Spek, *J. Organomet. Chem.* 511 (1996) 281.
- [30] P.P.M. de Lange, E. Alberts, M. van Wijnkoop, H.-W. Frühauf, K. Vrieze, H. Kooijman, A.L. Spek, *J. Organomet. Chem.* 465 (1994) 241.
- [31] M. Kokkes, D.J. Stufkens, A. Oskam, *J. Chem. Soc., Dalton Trans.* (1983) 439.
- [32] P.P.M. de Lange, M.J.A. Kraakman, M. van Wijnkoop, H.-W. Frühauf, K. Vrieze, W.J.J. Smeets, A.L. Spek, *Inorg. Chim. Acta* 196 (1992) 151.
- [33] R. Siebenlist, H.-W. Frühauf, K. Vrieze, W.J.J. Smeets, A.L. Spek, *Eur. J. Inorg. Chem.* (2000) 907–919.
- [34] E.H. Braye, W. Hübel, *Inorg. Synth.* 8 (1966) 178.
- [35] R. Isaksson, T. Liljefors, J. Sandstrom, *J. Chem. Res. (m)* (1981) 664.
- [36] R.N. Hurd, G.D. La Mater, G.C. McElheny, R.J. Turner, V.H. Wallingford, *J. Org. Chem.* 26 (1961) 3980.
- [37] H. Alper, A.S.K. Chan, *Inorg. Chem.* 13 (1974) 225.
- [38] J.L. Boer, A.J.M. Duisenberg, *Acta Crystallogr., Sect. A* 40 (1984) 410.
- [39] A.L.J. Spek, *Appl. Crystallogr.* (1988) 578.
- [40] N. Walker, D. Stuart, *Acta Crystallogr., Sect. A* 39 (1983) 158.
- [41] G.M. Sheldrick, SHELXS86, Program for Crystal Structure Determination, University of Göttingen, Göttingen, Germany, 1986.
- [42] P.T. Beurskens, G. Admiraal, G. Beurskens, W.P. Bosman, S. Garcia-Granda, R.O. Gould, J.M.M. Smits, C. Smykalla, The DIRDIF Program System, Technical Report of the Crystallography Laboratory, University of Nijmegen, Nijmegen, The Netherlands, 1992.
- [43] G.M. Sheldrick, SHELXL-93, Program for Crystal Structure Determination, University of Göttingen, Göttingen, Germany, 1993.
- [44] H.D. Flack, *Acta Crystallogr., Sect. A* 39 (1983) 876.
- [45] A.J.C. Wilson, *International Tables for Crystallography*, Kluwer Academic Publishers, Dordrecht, The Netherlands, 1992.
- [46] A.L. Spek, *Acta Crystallogr., Sect. A* 46 (1990) C34.
- [47] J.M.M. Smits, H. Behm, W.P. Bosman, P.T. Beurskens, *J. Crystallogr. Spectrosc. Res.* 18 (1991) 447.
- [48] D.T. Cromer, J.B. Mann, *Acta Crystallogr., Sect. A* 24 (1968) 321.
- [49] D.T. Cromer, J.B. Mann, *International Tables for Crystallography*, vol. IV, Kynoch Press, Birmingham, UK, 1974, p. 55.
- [50] S.R. Hall, H.D. Flack, J.M. Stewart, X-TAL3.2 Reference Manual, Universities of Western Australia, Geneva and Maryland, 1992.
- [51] H.W. Frühauf, A. Landers, R. Goddard, C. Krüger, *Angew. Chem., Int. Ed. Engl.* 17 (1978) 64.
- [52] L.H. Staal, L. Polm, R.W. Balk, G. van Koten, K.K. Vrieze, A.M.F. Brouwer, *Inorg. Chem.* 19 (1980) 3343.
- [53] L.H. Staal, G. van Koten, K. Vrieze, *J. Organomet. Chem.* 206 (1981) 99.
- [54] R. Zoet, G. van Koten, G. Muller, K. Vrieze, M. van Wijnkoop, K. Goubitz, C.J.G. van Halen, C.H. Stam, *Inorg. Chim. Acta* 149 (1988) 193.
- [55] R. Siebenlist, H.-W. Frühauf, K. Vrieze, H. Kooiman, W.J.J. Smeets, A.L. Spek, *Organometallics* 19 (2000) 3016.
- [56] C.H. Wei, L.F. Dahl, *Inorg. Chem.* 4 (1964) 1.
- [57] R. Siebenlist, H.-W. Frühauf, K. Vrieze, N. Veldman, A.L. Spek, unpublished.
- [58] R. Siebenlist, M. de Beurs, N. Feiken, H.-W. Frühauf, K. Vrieze, H. Kooiman, N. Veldman, M.T. Lakin, A.L. Spek, *Organometallics* 19 (2000) 3032.
- [59] F. Muller, D.I.P. Dijkhuis, G. van Koten, K. Vrieze, D. Heijdenrijk, M.A. Rotteveel, C.H. Stam, M.C. Zoutberg, *Organometallics* 8 (1989) 992.
- [60] F. Muller, G. van Koten, M.J.A. Kraakman, K. Vrieze, R. Zoet, K.A.A. Duineveld, D. Heijdenrijk, C.H. Stam, M.C. Zoutberg, *Organometallics* 8 (1989) 982.
- [61] L.H. Staal, G. van Koten, K. Vrieze, B. van Santen, C.H. Stam, *Inorg. Chem.* 20 (1981) 3598.

- [62] G.J. Kruger, A.v.A. Lombard, H.G. Raubenheimer, J. Organomet. Chem. 331 (1987) 247.
- [63] J. Meunier-Piret, P. Piret, M. van Meersche, Acta Crystallogr. 19 (1965) 85.
- [64] Y. Chauvin, D. Commereuc, D. Hugo, A. de Cian, R.E. Weiss, Nouveau J. Chim. 3 (1979) 183.
- [65] H. Alper, D.A. Brandes, Organometallics 10 (1991) 2457.
- [66] J. Messelhäuser, I.-P. Lorenz, K. Haug, W. Hiller, Z. Naturforsch. 40b (1985) 1064.
- [67] H.P. Weber, R.F. Bryan, J. Chem. Soc. (A) (1967) 182.
- [68] J.A. Adeleke, Y.-W. Chen, L.-K. Liu, Organometallics 11 (1992) 2543.
- [69] H.-W. Frühauf, F. Seils, C.H. Stam, Organometallics 8 (1989) 2338.
- [70] R.R. Holmes, in: S.J. Lippard (Ed.), Progress in Inorganic Chemistry, Wiley, Cambridge, MA, 1984, pp. 119–236.
- [71] A.R. Rossi, R. Hoffmann, Inorg. Chem. 14 (1975) 365.
- [72] E. Lindner, C.-L. Krieg, W. Hiller, R. Fawzi, Angew. Chem. 96 (1984) 508.
- [73] H. Kisch, C. Krüger, H.E. Marcolin, A.X. Trautwein, Z. Naturforsch. 42b (1987) 1435.
- [74] H. tom Dieck, R. Diercks, L. Stamp, H. Bruder, T. Schuld, Chem. Ber. 120 (1987) 1943.
- [75] F.H. Allen, O. Kennard, D.G. Watson, L. Brammer, A.G. Orpen, R. Taylor, J. Chem. Soc., Perkin Trans. II (1987) S1.
- [76] W.P. Mul, C.J. Elsevier, H.-W. Frühauf, K. Vrieze, I. Pein, M.C. Zoutberg, C.H. Stam, Inorg. Chem. 29 (1990) 2336.
- [77] M. Kokkes, D.J. Stufkens, A. Oskam, J. Chem. Soc., Dalton Trans. (1984) 1005.
- [78] H.K. van Dijk, D.J. Stufkens, A. Oskam, J. Am. Chem. Soc. 111 (1989) 541.
- [79] T.A. Manuel, T.J. Meyer, Inorg. Chem. 7 (1964) 1049.
- [80] R.B. King, P.M. Treichel, F.G.A. Stone, J. Am. Chem. Soc. 83 (1961) 3600.
- [81] D.J. Darensbourg, H.H. Nelson, C.L. Hyde, Inorg. Chem. 13 (1974) 2135.
- [82] D. Leibfritz, H. tom Dieck, J. Organomet. Chem. 105 (1976) 255.
- [83] L.H. Staal, L. Polm, K. Vrieze, Inorg. Chim. Acta 40 (1980) 165.
- [84] R.S. Berry, Chem. Phys. 32 (1960) 993.
- [85] L.H. Staal, J. Keijsper, L. Polm, K. Vrieze, J. Organomet. Chem. 204 (1981) 101.
- [86] H.-W. Frühauf, F. Seils, R.J. Goddard, M.J. Romão, Organometallics 4 (1985) 948.
- [87] H.-W. Frühauf, F. Seils, J. Organomet. Chem. 302 (1986) 59.
- [88] M. Hesse, H. Meier, B. Zeeh, Spectroskopische Methoden in der Organischen Chemie, Georg Thieme Verlag, Stuttgart, New York, 1984.
- [89] H.-W. Frühauf, J. Breuer, J. Organomet. Chem. 277 (1984) C13.
- [90] R. Hoffmann, Science 211 (1981) 995.
- [91] R. Hoffmann, Angew. Chem., Int. Ed. Engl. 21 (1982) 711; Angew. Chem. 94 (1982) 725.
- [92] R. Huisgen, 1,3-Dipolar Cycloaddition Reactions, Wiley, New York, 1984.